ABSTRACT

BETTY L. GATANO. Determining the Transfer Efficiency of a HVLP Spray Gun (Under the direction of DR. MICHAEL R. FLYNN)

In this work, a mathematical relationship between the transfer efficiency of a high volume low pressure (HVLP) spray gun and its operational parameters was developed. Spray paint operations were simulated by a mannequin spraying a nonvolatile oil from the HVLP gun onto a flat plate. The transfer efficiency was calculated from the amount of oil sprayed from the gun and the amount impacted on the plate. Mannequin motion and orientation, air pressure of the spray gun, and air velocity in the wind tunnel were varied to assess their effect on transfer efficiency. The measured transfer efficiencies ranged from 0.66 to 0.87. Transfer efficiency decreased linearly as a function of the mass of air to the mass of liquid sprayed (m_a/m_l). Mannequin motion also decreased the transfer efficiency at the highest values of m_a/m_l.

A theoretical model for predicting transfer efficiency based on the inertial impaction of particles onto a workpiece was also developed. Although the model over estimated the transfer efficiencies, good agreement was noted between the predicted transfer efficiencies and measured values. The theoretical model has the potential to be a useful tool for estimating concentrations of liquid mists in a worker's breathing zone.

ACKNOWLEDGMENTS

This work would have not been possible without the financial support of NIOSH grant #5R01 OH02858, "Computational Methods in Industrial Ventilation."

Many people contributed to the completion of this report. First of all, I owe many thanks to my advisor, Dr. Michael Flynn, whose support, understanding, and guidance was appreciated more than I can say here. Also, I want to thank Dr. David Leith and Dr. Michael Symons for reading my report and providing their invaluable input.

Three people were especially important in helping me finish this report. I owe a big debt to John McKernan, my lab partner and friend. Without him, I *never* would have understood how to hook up that spray gun. His patience and support during my numerous panic attacks were much appreciated. I also want to thank Jordan Kovitz for his work in developing the inertial impaction model and for trying time and time again to explain it to me. Finally, I want to thank Kevin Dunn for always answering my questions about spray painting and making me laugh at the same time.

There are many more people that I want to acknowledge. I would like to thank everyone in the Baity Laboratory (especially for all their help today when my computer ate my thesis). Thanks also to Kendall and Laurie for their friendship during my time in graduate school. I owe a big thanks to Nancy for everything that she did for me the past two years. Thanks for the cookies! Lastly, I want to thank my best friend, Carolyn, who has always encouraged me to do more than I ever thought I could. E.D.O.B!

The most important people to me and the ones who deserve the biggest thanks are my parents and sisters. They believed in me even when I didn't believe in myself. They have my thanks and love forever.

TABLE OF CONTENTS

LIST OF TABLES

LIST OF FIGURES

LIST OF SYMBOLS

A_{cap}	area of air discharge of cap (square feet)
B	breadth of worker (ft)
C	Concentration in a worker's breathing zone (mg/m^3)
C_c	Cunningham correction factor (unitless)
D_{nozzle}	diameter of hypothetical nozzle and distance from the hypothetical nozzle to the workpiece (m)
d_{50}	impactor cut size (m)
g_c	gravitational constant of 32.174 ft-lb/lb_f-s^2
H	height of worker (ft)
K	kinematic momentum (m^4/s^2)
m	superscript used in Kim and Marshall Equation (unitless)
m_a, m_l	masses of air and liquid, respectively (lb/min)
m_{gun}	mass of air from gun, based on cap and horn (kg/s)
MMD	mass median diameter (μm)
p, p_n	nozzle pressure (lb_f/ft^2)
p_o	pressure in reservoir (lb_f/ft^2)
Q_{jet}	volumetric flowrate from circular jet (m^3/s)
Re	Reynolds number (unitless)
STK_{50}	Stokes number corresponding to 50% collection efficiency of an impactor (unitless)
TE_{pred}, TE_{mes}	predicted and measured transfer efficiency, respectively (unitless)
U_{fs}	air velocity of the wind tunnel (ft/s)
U_{gun}	velocity of air from HVLP spray gun (m/sec)
U_{rel}	relative velocity of air to liquid from spray gun (ft/sec)
U_{nozzle}	velocity of air at hypothetical nozzle (m/s)
X	distance downstream from the hypothetical circular jet (m)
x^*	reduced diameter, d_{50}/MMD
Y	distance downstream from the circular jet to the workpiece (m)

LIST OF SYMBOLS (continued)

Greek Letters

σ	surface tension of liquid (dynes/cm)
Φ_v	cumulative volume frequency for a particle size distribution (unitless)
μ_a, μ_l	viscosities of air and liquid, respectively (centipoise)
γ	ratio of specific heats: constant at 1.4 for air (unitless)
ρ_a, ρ_l	densities of air and liquid, respectively (lb/ft^3)
ρ_{air}	particle of air from spray gun (kg/m^3)
ρ_p	particle density (kg/m^3)
ρ_o	density of air in the reservoir (lb/ft^3)

I. INTRODUCTION

The high volume low pressure (HVLP) spray gun is a specialized piece of spray painting equipment that operates at lower gun pressures and produces greater air flowrates than conventional spray guns. While conventional guns operate at typical cap pressures in the range of 50 to 60 psig, the HVLP spray gun is limited to a maximum of 10 psig at the gun cap. Air flowrates for the HVLP spray gun can exceed 20 scfm at 10 psig. Conventional guns only produce around 14 to 16 scfm at their maximum pressure range.[1]

HVLP spray guns have also been reported to have higher transfer efficiencies than conventional spray guns.[1] The transfer efficiency of a spray gun represents the fraction of mass sprayed from the gun that deposits onto the workpiece. Droplets not deposited onto the workpiece are termed overspray and have the potential to be transported into the worker's breathing zone. Thus, spray guns with higher transfer efficiency, such as the HVLP gun, have lower rates of overspray and a reduced potential for worker exposure to mists.

Recent work has documented the relationship between transfer efficiency and worker exposure.[2, 3] Carlton and Flynn (1996) have developed a model that predicts the concentration of particles in a worker's breathing zone as a function of the overspray generation rate. Heitbrink et. al. (1996) have shown experimentally that the higher transfer efficiencies associated with HVLP guns correspond to lower worker exposure to paint mists as compared to the transfer efficiencies of a conventional spray gun.

From an environmental perspective, higher transfer efficiencies can reduce the amount of paint consumed and the amount of volatile organic compounds (VOCs) emitted from spray paint operations.[1] For these reasons, HVLP guns can be used as control technology. One such case is in the State of California, which requires that HVLP spray guns (or other spray equipment capable of achieving a 65% transfer efficiency) be used in surface coating applications.[1, 4]

Because of the potential benefits of achieving higher transfer efficiencies in spray painting operations, methods for quantifying transfer efficiency may be important to spray paint operators, environmental managers, and others. The objectives of this work were to

examine the factors that affect transfer efficiency and to develop a theoretical model to predict transfer efficiency based on the inertial impaction of particles onto a workpiece.

II. THEORETICAL CONSIDERATION

The application of paint from a spray gun to a surface can be modeled as an impaction process. Initially, a spray gun atomizes liquid into droplets, which are then transported to a workpiece via momentum of the air jet. Paint droplets with sufficient inertia impact upon and coat the workpiece, while particles with less inertia follow the airstream and become part of the overspray. From this simplified overview of the coating process, a model was developed to predict the transfer efficiency of the HVLP spray gun. The various steps of the impaction model - atomization, transport via momentum, impaction, and overspray - are discussed in detail in this section.

2.1 Atomization

The performance of an atomizer, such as the HVLP spray gun, depends on its size, the geometry of the nozzle, the physical properties of the liquid being atomized, and the medium enveloping the atomized liquid.[5]

Because of the low pressures associated with a HVLP spray gun, its geometry may be more critical in atomization than that of a conventional spray gun.[1, 6] Figure 1 shows a schematic of the HVLP spray gun nozzle. As seen in the figure, air is discharged through an annulus surrounding the liquid nozzle. Atomization of liquid from the HVLP spray gun occurs as the stream of liquid is discharged into the surrounding column of relatively fast moving air. Because two fluids are involved, this type of atomization is termed twin-fluid atomization. The HVLP gun is referred to as an external-mixing atomizer, meaning that the high velocity air stream impinges on the liquid outside the liquid discharge nozzle.[5]

Two of the most important liquid properties affecting atomization are surface tension and viscosity. Surface tension is a cohesive force that resists the disintegration of

liquid into smaller droplets. Viscosity affects both the drop size distribution and the flowrate of liquid. An increase in viscosity will decrease the Reynolds number (Re) and prevent instabilities in the liquid jet. Disintegration of the liquid occurs when aerodynamic forces exceed these consolidating forces.[5]

The particle size distribution of liquid droplets atomized by the HVLP spray gun defines the fraction of particles that will impact a workpiece. Since the atomization process is complex, prediction of particle size distributions results primarily from empirical correlations.[5] One such correlation, developed by Kim and Marshall (1971), was used here to predict the mass median diameter (MMD) of the particle size distribution. The following equation presents the Kim and Marshall correlation[7]:

$$MMD = 249\left[\frac{\sigma^{0.41}\ \mu_l^{0.32}}{\left(U_{rel}^2\ \rho_a\right)^{0.57} A_{cap}^{\ 0.36}\ \rho_l^{0.16}}\right] + 1260\left(\frac{\mu_l^2}{\rho_l\ \sigma}\right)^{0.17} \frac{1}{U_{rel}^{0.54}} \left(\frac{m_a}{m_l}\right)^m \quad (1)$$

The Kim and Marshall model correlates the MMD from a spray gun to physical properties of the liquid and air, the relative velocity between the two fluid streams, the area of the air nozzle, and the ratio of the mass of air to mass of liquid sprayed.[7]

As seen in Figure 1, the HVLP spray gun can discharge air from both its horns and its cap. However, only the air flow from the annular nozzle in the cap was assumed to atomize the liquid. Flow from the horns was assumed to determine the spray pattern. Applying the Kim and Marshall correlation to predict the particle size distribution required that a distinction be made between the two air flows. Thus, only the parameters associated with air flow from the cap were used in Equation 1.

Since a direct measurement of the air flow from the cap was difficult, the mass flowrate of air through the cap was estimated from the velocity in the cap. Assuming that the flow from the nozzle is frictionless and subsonic, the following equation can be used to calculate the velocity[8]:

$$u = \left[\frac{2 \gamma g_c p_o}{(\gamma - 1)\rho_o} \left[1 - \left(\frac{p}{p_o} \right)^{(1-1/\gamma)} \right] \right]^{0.5} \quad (2)$$

The reservoir density of air (ρ_o) in the above equation was calculated from the power law relationships for compressible flow through a nozzle.[9]

Air velocity for both the cap and the horns was calculated from Equation 2 for the range of experimental pressures. Mass flowrates were then estimated based on these velocities, the air discharge areas of the cap and horns, and the density of air when discharged. The resulting mass flowrate of air was shown to be divided equally between the cap and the horns. Thus, the mass flowrate term (m_a) as used in Equation 1 was estimated as half the total mass of air from the HVLP spray gun.

2.2 Momentum

Air flow from the HVLP spray gun was modeled as an equivalent momentum air flow discharged from a circular orifice. As the air jet increases in distance from its discharge orifice, the mass of air in the jet increases and the air velocity decreases. Consequently, the momentum of the air jet remains constant. Using this principle of constant momentum and ignoring the presence of particles in the airstream, the volumetric flowrate of air can be predicted at a some distance, X, downstream from the jet. The volumetric flowrate of a jet at point X is given as the following[10].

$$Q_{jet} = 0.404 \cdot X \cdot \sqrt{K} = 0.404 \cdot X \cdot \sqrt{\frac{m_{gun} U_{gun}}{\rho_{air}}} \quad (3)$$

Since the momentum of the HVLP spray gun depends on air flow from the horns and the cap, the total mass flowrate of air from the HVLP spray gun was used in Equation 3.

Since the circular jet does not exist in reality, it is represented by the hypothetical jet shown in Figure 2. The location of the hypothetical jet with respect to the workpiece

(referred to as distance Y in Figure 2) was determined from basic trigonometry, given the spray pattern of particles on the workpiece and the spray angle from the hypothetical jet. Spray angles from circular jets are reported in literature, and a value of 29° was used here.[11] The actual spray pattern formed by the HVLP gun was elliptical and differed from the circular pattern that would be formed by the hypothetical jet. To compensate for this difference, the spray pattern from the HVLP gun was modeled as if it were a circle having an equivalent area as the ellipse. The radius of the modeled circle was used, along with the spray angle, to calculate the location of the hypothetical jet.

2.3 Impaction

When an object is placed in the path of an air stream thereby causing the stream to change directions, any particles with sufficient inertia will follow their original path and impact upon the object. Particles with less inertia will follow the air path. For an ideal impactor, a particle size exists that represents the point where half of the particles impact and half pass along with the air stream. This particle size is referred to as the cut size or d_{50} of an impactor and can be calculated from the following equation[12]:

$$d_{50} = \left[\frac{9 \ \mu_a \ D_{nozzle} \ (STK_{50})}{\rho_p \ U_{nozzle} \ C_c} \right]^{0.5} \qquad (4)$$

Using Equation 4 to calculate the d_{50} for the HVLP spray gun required that assumptions be made regarding the particle size distribution and the air flow. The Cunningham correction factor in Equation 4 was assumed to equal 1. The air flow was assumed to be in the Stokes regime (i.e., 500 < Re <3000). With this assumption, the theoretically derived Stokes number corresponding to 50% collection efficiency (i.e. STK_{50}) could be used. The STK_{50} is 0.24 for circular jets.[12]

The impaction of particles onto the workpiece can be modeled as if the air stream from the HVLP spray gun was discharged from an impactor nozzle. Since this impactor nozzle does not exist in reality, it is represented by a hypothetical nozzle, as shown in Figure 2. The distance from the hypothetical jet to the hypothetical nozzle (referred to as distance x in Figure 2) was based on the diameter of the hypothetical nozzle. The diameter and the distance from the hypothetical nozzle to the work piece (Y-x) were set equal, and the lengths were determined from iterative calculations.

Once the distance from the hypothetical jet to the hypothetical nozzle is known, then the velocity of the air stream at the hypothetical nozzle can be calculated from the volumetric flowrate given in Equation 3 and the area of the hypothetical nozzle. The cut size of the particles impacting the workpiece are calculated from Equation 4, given the calculated velocity.

2.4 Overspray

Kim and Marshall (1971) determined that the cumulative volume frequency of the particle size distribution from a twin-fluid spray gun was log normally distributed and could be described by the following logistic equation[7]:

$$\Phi_v = \frac{1.15}{1 + 6.67 \exp\left(-2.18\ x^*\right)} - 0.15 \qquad (5)$$

Assuming that the density of particles is constant, Equation 5 also represents the cumulative mass frequency.

The x^* term in the above equation is the reduced diameter, which is defined as the ratio of the particle diameter to the mass median diameter of the size distribution. When the d_{50} is used in the reduced diameter, then Φ_v represents the fraction of particles smaller than the d_{50} that will not impact the workpiece. In other words, the Φ_v defines the

overspray fraction. Transfer efficiency, or the fraction of particles impacting the workpiece, is simply 1 - Φ_v .

III. METHODOLOGY

3.1 Laboratory Set Up

A laboratory model of a spray painting operation was used to determine the transfer efficiency of the HVLP spray gun. The model consisted of a mannequin spraying vacuum pump oil with the HVLP spray gun. The mannequin was automated so that its arm could be stationary or in motion while it sprayed. Spraying occurred in a wind tunnel that represented a paint spray booth. The wind tunnel was 5-feet-by-5-feet with a resulting cross-sectional area of 25 square feet. The depth of the wind tunnel was 8 feet. Flared entrance flanges and a pegboard on the rear wall of the wind tunnel created a uniform velocity profile. A bank of disposable particle filters mounted on the rear pegboard helped to establish an uniform air velocity profile in the wind tunnel, while providing a mechanism for cleaning the exhausted air.

The gun used in the spray painting operations was a DeVilbiss MSV-533-4-FF model HVLP spray gun fitted with a #33A air cap. This pneumatic, external-mixing spray gun operated at pressures from 0.1 to 10 psig, as measured at the nozzle cap. A two-stage compressor pump provided pressurized air for the spray gun. The pressurized air was fed to a galvanized steel pot, where the liquid to be sprayed was pressurized to 10 psig. Air pressures in the pot ranged from 16 to 53 psig, depending on the required cap pressure. The air pressure was reduced to the required cap pressure within the gun. Figure 3 shows a schematic of the pressurized pot.

The HVLP gun allows for fan pattern to be varied by adjusting the amount of air emitted for the gun's horns. For this work, a realistic fan pattern was selected and remained constant for the duration of the experiment. The resulting fan pattern was a 2:1 ellipse, approximately 9 inches in length.

Vacuum pump oil was used to simulate the paint, which could not be used in this experiment due to the explosion potential associated with the paint solvents. Instead, vacuum pump oil was selected because it is nonvolatile, inexpensive, and has physical properties similar to paint. The liquid viscosity of the vacuum pump oil was dependent on temperature and ranged from around 64 to 68 centipoise throughout the experiment. The surface tension of the oil was not available from the manufacturer but was estimated as 40.7 dynes/cm.

The mannequin used in the experiment stood 51 inches high and measured 14 inches across the chest. The mannequin was not anthropometric but was truncated at the thighs to fit in the wind tunnel. As shown in Figure 4, mannequin orientation in the wind tunnel was either parallel (180°) or perpendicular (90°) with the air flow in the wind tunnel. In both orientations, the mannequin was placed at a depth of 48 inches in the wind tunnel. In the 180° position, the 48 inches was measured from the mannequin's back to the front of the wind tunnel. In the 90° position, the 48 inches was measured from the center of the mannequin's leg to the front of the wind tunnel.

The HVLP spray gun was placed in the mannequin's right (downstream) hand, eight inches from a flat plate. The flat plate created a uniform air jet rebound and formed a reproducible overspray generation rate. When the mannequin was stationary, the spray pattern was centered on a flat plate 3 feet in height by 2 feet in width. A larger plate was required when the mannequin was in motion because, as the mannequin moved the spray gun horizontally across the plate, the path of the mannequin's arm exceeded the width of the smaller plate. A 3-by-3-foot flat plate was used to assess motion.

A collection trough was located underneath the plate. Oil sprayed onto the plate drained into the trough. A squeegee was used to remove any residual from the plate. The difference in trough weight before and after spraying determined the mass transferred to the plate, and this value was used to calculate the transfer efficiency.

3.2 *Experimental Design*

Prior to beginning the experiment, all instruments were calibrated to ensure accurate and reproducible results. Appendix A summarizes the calibrations performed on all the necessary equipment.

Four experimental parameters - mannequin motion, mannequin orientation, cap pressure, and air velocity of the wind tunnel (i.e., freestream velocity) - were varied to assess their effect on transfer efficiency. For the effect of motion, the mannequin was evaluated as either in motion or stationary. The speed of the mannequin's arm was established as approximately 8.25 cycles per minute and was determined experimentally as a rate that was realistic for an actual spray paint operation. Mannequin orientation was parallel (180°) or perpendicular (90°) to the wind tunnel freestream, as seen in Figure 4. The velocity of the wind tunnel freestream was varied in tandem with the cap pressure, and Table 1 shows the variations of cap pressures and freestream velocities. Pressures from the HVLP spay gun varied from 1.5 to 6.5 psig*, as measured at the nozzle cap. Values for freestream velocity represented values typical of velocities encountered in the field and scaled to the mannequin height. As seen in the table, the nozzle pressures and velocities differed depending on mannequin motion. Motion caused overspray to escape from the front of the wind tunnel at cap pressures of 6 and 6.5 psig. To correct for this effect and eliminate redundant measurements, the velocity of the wind tunnel was increased for the highest cap pressure, and the set of runs based on cap pressures of 6 psig was eliminated when the mannequin was in motion.

---

* The HVLP spray gun can attain a maximum pressure of 10 psig measured at the nozzle cap. Because of physical limitations of the wind tunnel, this maximum value was not attainable during the experimentation. At higher cap pressures, the overspray escaped from the wind tunnel. This phenomenon was especially predominate during motion runs, and the velocity of the wind tunnel was increased accordingly.

Table 1. Overview of Nozzle Pressure and Freestream Velocity*

No Motion		Motion	
Nozzle Pressure (psig)	Velocity (ft/s)	Nozzle Pressure (psig)	Velocity (ft/s)
1.5	150	1.5	150
2.5	125	2.5	125
4.25	100	4.25	100
6.0	7.5	–	–
6.5	75	6.5	100

* As measured at the nozzle cap

IV. RESULTS

4.1 Experimental Results

Appendix A contains the experimental measurements for the transfer efficiency. All statistical analyses were performed by either the SAS program or the data analysis tool in Excel. The results of the analyses are included in Appendix B.

The transfer efficiency for the HVLP spray gun ranged from 0.66 to 0.87 over all model runs. Table 2 presents the mean transfer efficiencies for "Motion" and "No Motion."

As noted in Equation 1, the ratio of air to liquid mass flowrates (m_a/m_l) from the spray gun is a factor in liquid atomization and, therefore, should be related to transfer efficiency. Figure 5 shows this relationship as determined from the experimental measurements. Since the m_a/m_l affects atomization, the values of m_a/m_l shown in the figure are based solely on the mass flowrate of air from the cap. As seen in the figure, the transfer efficiency decreases linearly with increasing m_a/m_l. The least square regression lines for the transfer efficiency are given in Table 2 and are categorized by motion. Transfer efficiency for the "Motion" case tended to be lower than the transfer efficiency for the "No Motion" case at the highest m_a/m_l. The two lines appear to converge as the m_a/m_l decreases. A partial F-test indicated that the slopes of the regression lines were significantly different at the 0.05 level ($p=0.0039$), while the intercepts were not

significantly different (p=0.0859). However, it should be noted that the m_a/m_l never reaches zero due to application limits of the spray gun. A practical lower limit of m_a/m_l was calculated and is shown in Figure 5. Additionally, the results of an analysis of variance (ANOVA) showed that neither the effect of orientation nor any interaction between orientation and motion were significant at the 0.05 level. Therefore, these terms were not included in the mathematical model for transfer efficiency and m_a/m_l.

Table 2. Regression Equations for Transfer Efficiency as a Function of m_a/m_l*

Run Type	Number of Runs	Linear Model	R^2
No Motion	36	TE = (-0.0928±0.01)*(m_a/m_l)+(0.966±0.018)	0.917
Motion	26	TE = (-0.122±0.017)*(m_a/m_l)+(0.998±0.033)	0.901

* at the $\alpha = 0.05$ confidence level.

4.2 Model Results

Appendix C contains the results of the impaction model and associated calculations. Since motion was not accounted for in the impaction model, transfer efficiencies were only calculated for the "No Motion" experimental runs. Calculated transfer efficiencies ranged from 0.74 to 0.90, and MMD calculated from Equation 1 ranged from 32.6 µm to 102.5 µm.

Figure 6 shows the measured transfer efficiency as a function of the predicted transfer efficiency. As seen in the figure, the impaction model tended to over estimate the transfer efficiency. The measured values of transfer efficiency are linearly correlated with the predicted values as expressed in following best fit regression equation:

$$TE_{meas} = 0.8518\ \left(TE_{pred}\right) + 0.1083, \qquad R^2 = 0.951$$

Based on the confidence intervals, the slope of the modeled regression line was shown to be statistically different than 1 ($p<0.001$), and the intercept was shown to be non-zero ($p=0.0003$).

V. DISCUSSION

5.1 Experimental Results

In this work, the transfer efficiency of a HVLP spray gun was shown to decrease linearly with increasing m_a/m_l. Figure 5 shows this relationship. Throughout this experiment, the mass of liquid sprayed from the gun was maintained at fairly consistent flowrate of approximately 115 grams/min. Consequently, the m_a/m_l was varied by varying the air pressure at the cap, which changed the mass flowrate of air from the gun. Increasing the cap pressure and the mass flowrate of air will reduce the MMD of the particle size distribution from the spray gun, as predicted by Equation 1. Since smaller particles have less inertia, they are less likely to impact the workpiece. Thus, increasing m_a/m_l from the spray gun increases the overspray fraction and reduces the transfer efficiency.

5.2 Limitations of the Relationship between m_a/m_l and Transfer Efficiency

The relationship between m_a/m_l and transfer efficiency was developed from a simplified version of actual spray paint operations. Even with the inclusion of motion in the experiment, the spray simulation was still limited. The actual transfer efficiency of an HVLP spray gun has been shown to depend on many factors not considered in this work. Such factors include the type of HVLP spray gun, the geometry and size of the target, the type of liquid being sprayed, and the skill of the painter.[4, 14] Thus, the relationship between m_a/m_l and transfer efficiency is specific to the spray system considered. Care must be taken when extrapolating the results presented in this work to wider applications.

5.3 Discussion of Impaction Model

The measured transfer efficiencies agree well with the predicted values, in spite of the gross generalizations of the model. However, the simple impaction model consistently over estimates the measured transfer efficiency. This tendency may reflect how the transfer efficiency measurements were made. Vacuum pump oil sprayed on the flat plate was allowed to drain into a trough located under the plate and any residual oil was squeegeed into the trough. Mass measurements for the transfer efficiency were then determined from differences in trough weight before and after spraying. Although care was taken to remove most of the oil from the plate, the system was not perfect. Some oil remained on the plate and the squeegee or was lost through minimal dripping. This loss may account for the differences between the actual and predicted values.

In practice, transfer efficiency is measured by weighing the liquid paint container and the workpiece before and after painting. Transfer efficiency can also be estimated by measuring the dry-film thickness of the paints.[15] These standard techniques were not applicable here because vacuum pump oil was used instead of paint or finish.

The simplified impaction model made several assumptions about the behavior of the HVLP spray gun. For example, the Cunningham correction factor in Equation 4 was assumed to equal 1. This assumption was acceptable because the calculated MMD were much larger than 1 μm. However, a violation in a basic assumption of the impaction model is that air flow from the HVLP spray gun is in the Stokes regime, with a Reynolds number of 3,000 or less. Under this assumption, a STK_{50} of 0.24 can be used to estimate the cut size of the hypothetical impactor. The Reynolds numbers were calculated and were showed to range from approximately 30,000 to 160,000. The effect of Reynolds number on the cut size is expected to be minimal. Studies have shown that efficiency curves for impactors are steeper at higher Reynolds numbers. Once the Reynolds number is above around 200, the effect of Reynolds number on the collection efficiency curve is

relatively small.[16] Thus, the actual value of the STK_{50} is not expected to differ greatly from 0.24 assumed in the impaction model.

5.4 Limitations of Impaction Model

The inertial impaction model represented a simplified version of actual spray paint operations. For example, consideration of motion was not included in the theoretical model nor was the effect of solvent volatilization. Consequently, the agreement between measured and predicted transfer efficiency may not be as good for real spray paint operations.

5.5 Implications of Impaction Model

The theoretical impaction model has a broader application than the mathematical relationship between m_o/m_l and transfer efficiency developed here. Although both the theoretical model and the mathematical relationship allow for prediction of transfer efficiency directly from operational parameters, only the theoretical model can be generalized to other HVLP spray painting systems. The mathematical relationship between m_o/m_l and transfer efficiency is specific only to the type of spray gun and liquid used in this work.

The theoretical model for transfer efficiency can be used with the concentration model developed by Carlton and Flynn for estimating the worker's breathing zone concentration of particle mists. Their model correlates the breathing zone concentration to the worker's height and breadth, his orientation with respect to the workpiece, cap pressure of the HVLP spray gun, liquid viscosity, freestream velocity, and the overspray generation rate.[2] A generalized form of their model is presented as follows:

$$\frac{CU_{fs}HB}{m_o} = \frac{CUHB}{m_l\ (1-TE)} = f\left(\frac{p_a\ \ H}{U_{fs}\ \ \mu_l}\right) \qquad (6)$$

With the exception of the overspray generation rate (m_o), the variables in the concentration model can be easily obtained from operational parameters and other measurements. The overspray generation rate can be calculated from the liquid flowrate when the transfer efficiency of the spray gun is known, as shown in the above equation. Thus, the inertial impaction model developed here has the potential to provide closure to the breathing zone concentration model so that a worker's exposure can be estimated from basic operational parameters of a spray system.

VI. CONCLUSIONS AND RECOMMENDATIONS

A strong mathematical relationship between the transfer efficiency of an HVLP spray gun and the m_s/m_l was developed in this work. The relationship indicates that transfer efficiency decreases linearly with increasing values of m_s/m_l. Motion was also shown to decrease the transfer efficiency. Factors not included in this research - such as the type of spray gun, the shape and size of the workpiece, the liquid viscosity, and the skill of spray paint operators - have been shown to influence transfer efficiency. Future field work may be useful to determine the strength of the relationship between transfer efficiency and m_s/m_l when these additional factors are taken into account.

A physical model for predicting transfer efficiency based on the inertial impaction of particles onto a workpiece was also developed. Although the model tended to over estimate the transfer efficiencies, good agreement was seen between the measured transfer efficiencies and those predicted by the impaction model. The theoretical model can be generalized to other HVLP spray systems and, as such, can provide closure to the concentration model developed by Carlton and Flynn. The theoretical model can be expanded to reflect more realistic spray painting applications in the future.

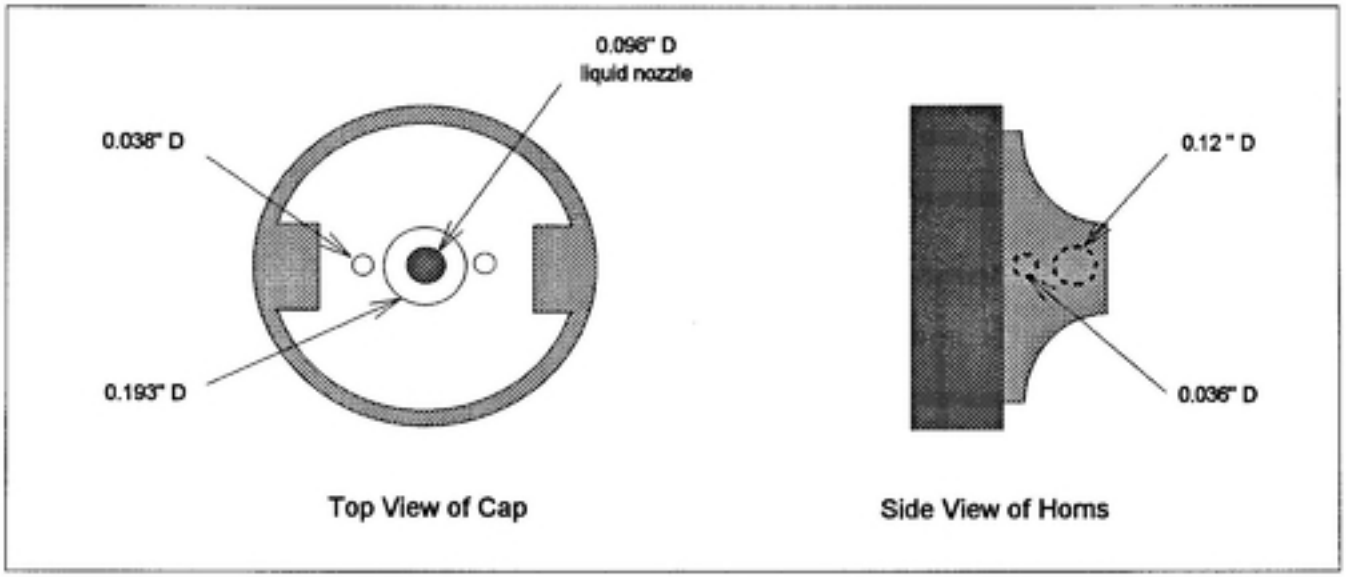

Figure 1. Schematic of HVLP Spray Nozzle (not drawn to scale)

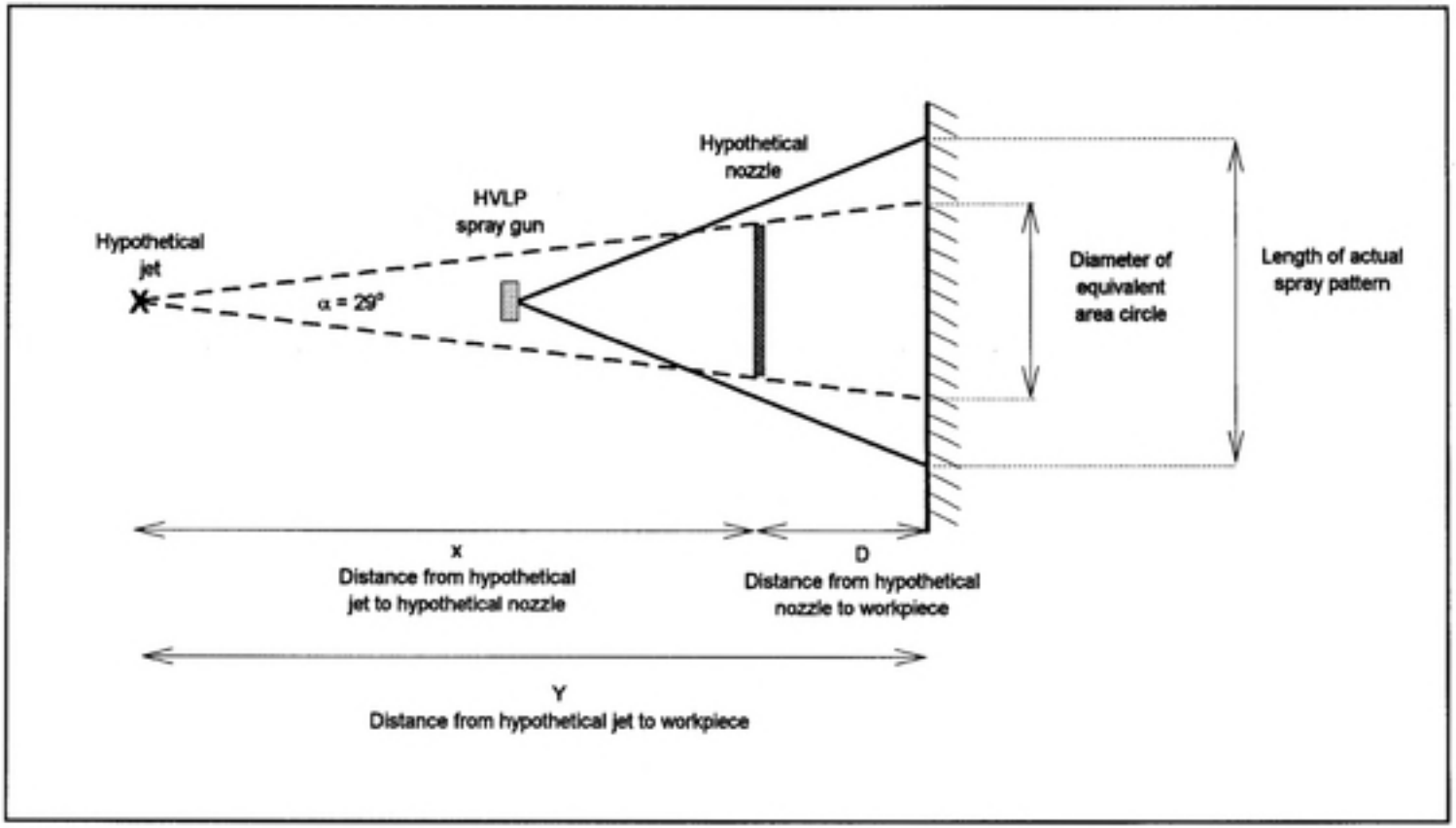

Figure 2. Schematic of Impaction Model (not drawn to scale)

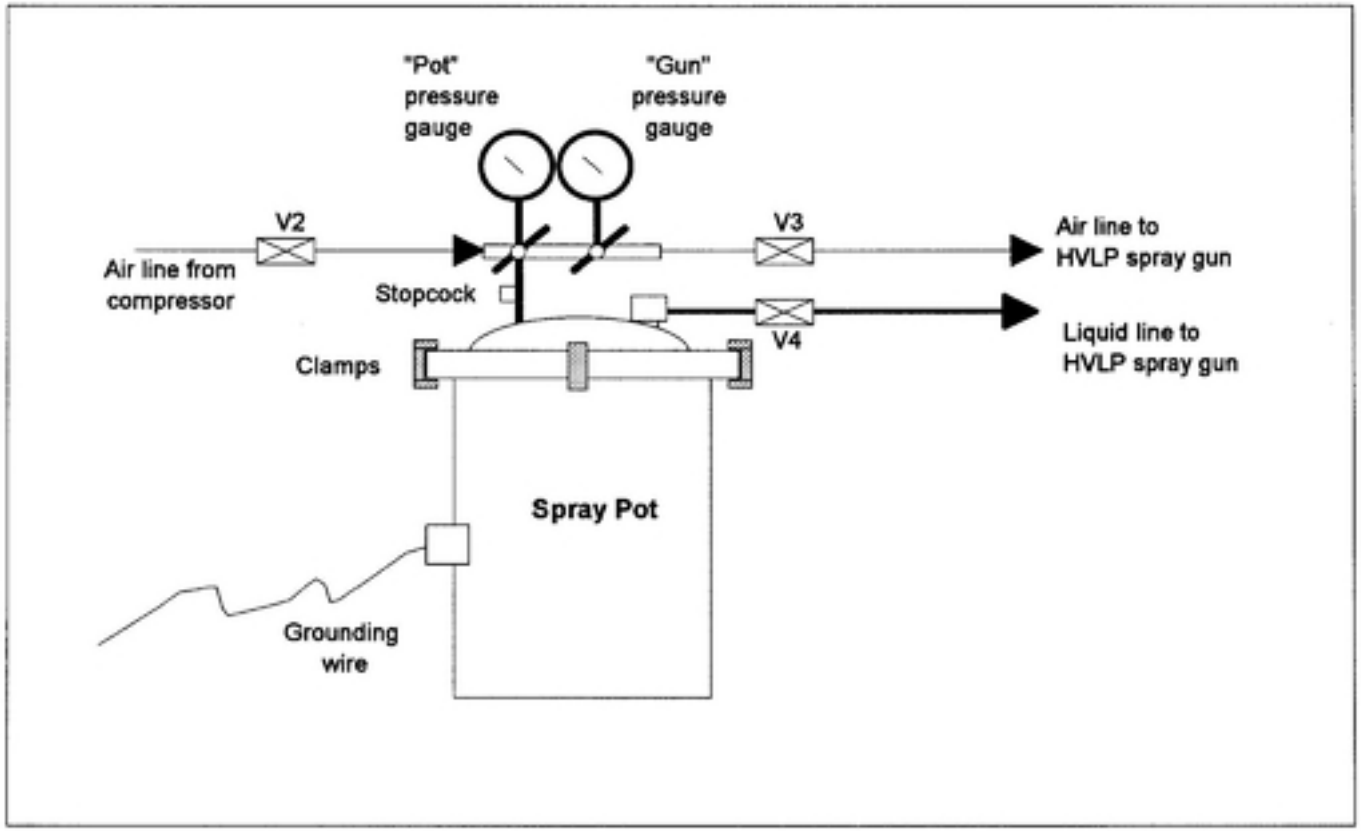

Figure 3. Schematic of Spray Pot System
(not drawn to scale)

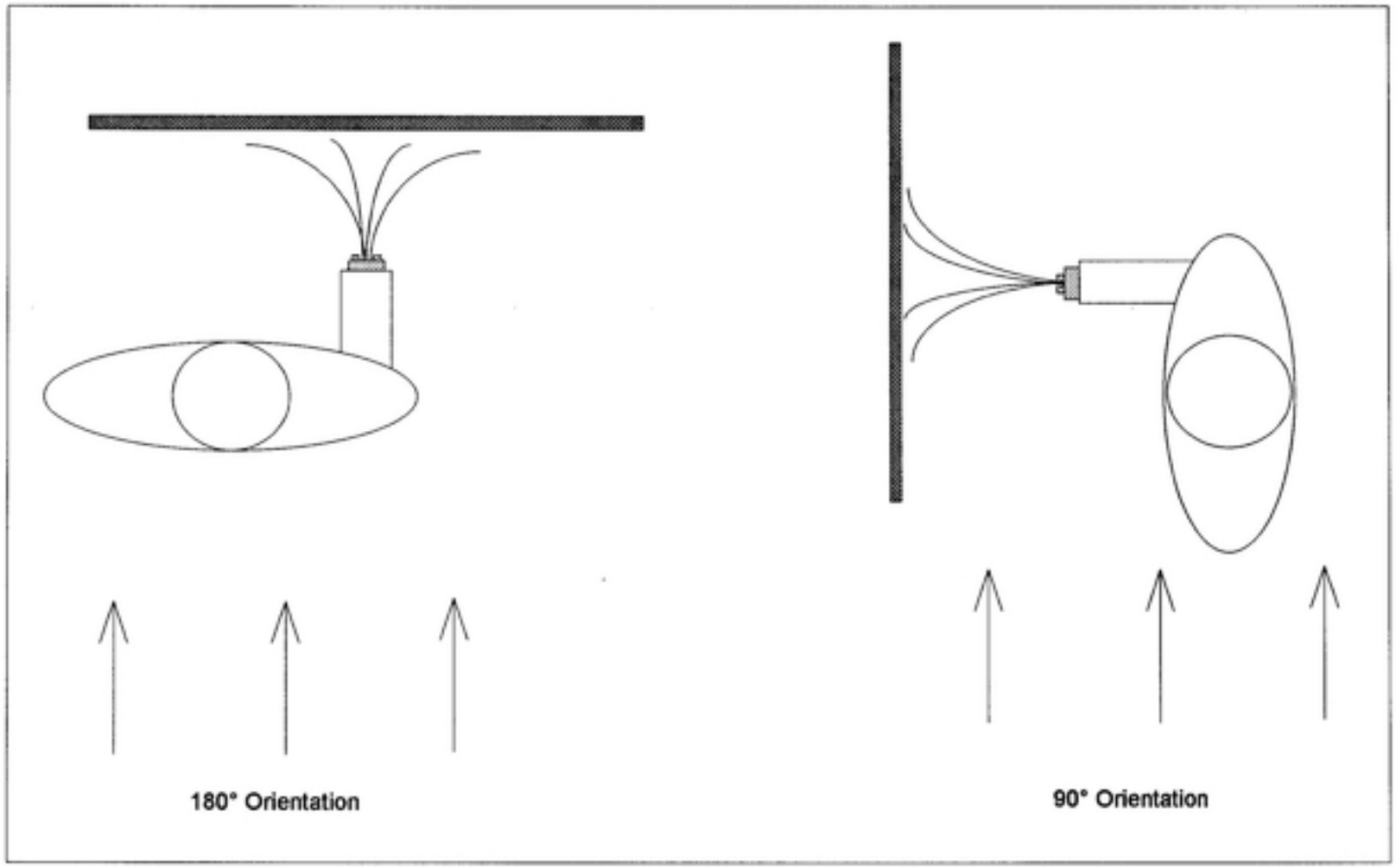

Figure 4. Orientation of Mannequin with Freestream

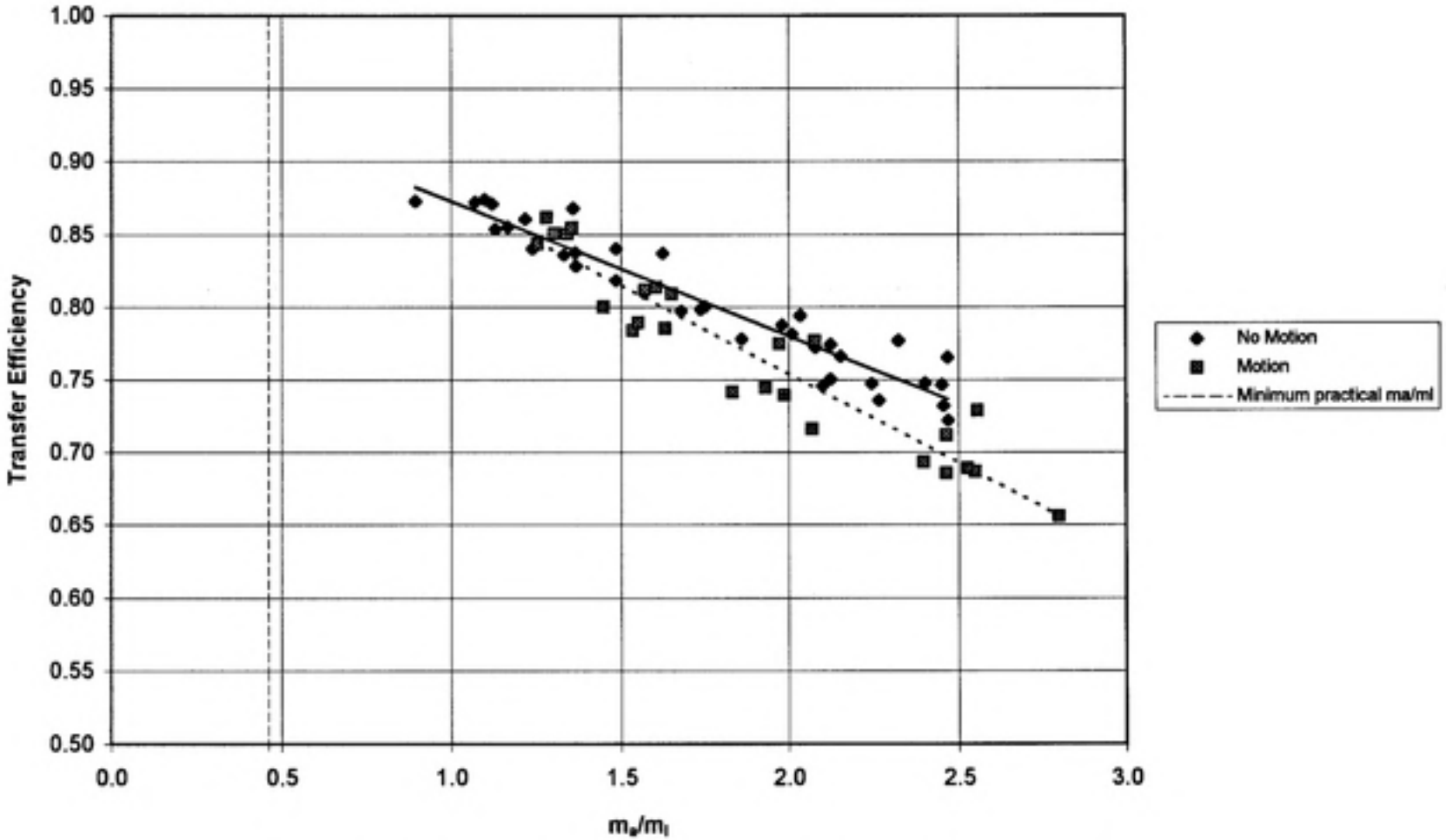

Figure 5. Transfer Efficiency as a Function of the Mass of Air to Mass of Liquid Ratio (m_a/m_l)

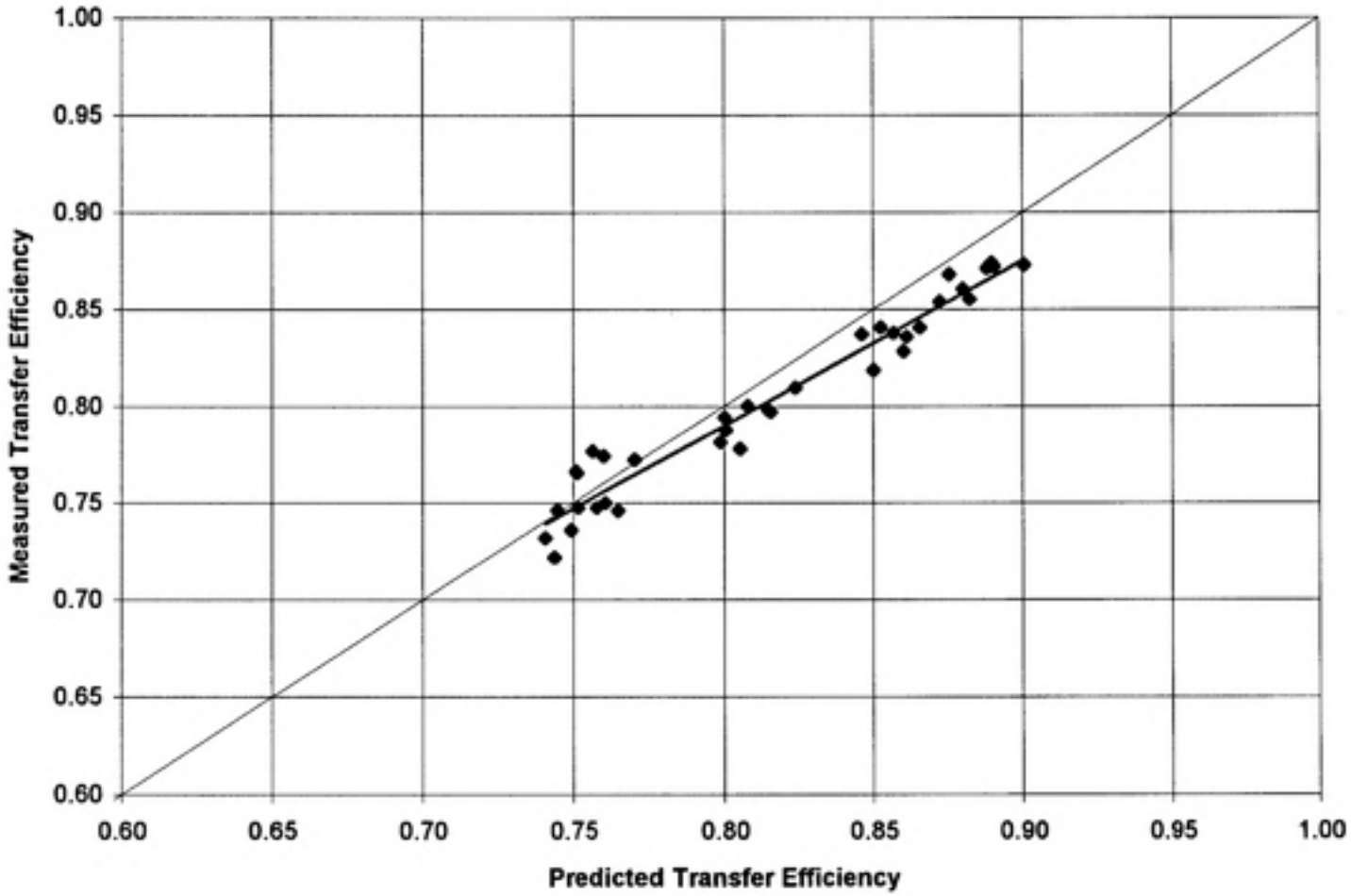

Figure 6. Measured Transfer Efficiency Compared to Predicted Transfer Efficiency Estimated from the Inertial Impaction Model

VII. REFERENCES

1. Cerdoz, R. and Treuschel, J. "HVLP, the 'Wonder' Gun." Industrial Finishing: Coatings Manufacturing and Application. Brochure. (1993).
2. Carlton, G.N and M.R. Flynn. "A Model to Estimate Worker Exposure to Spray Paint Mists." Submitted for publication to Appl. Occup. Environ. Hyg.
3. Heitbrink, W.A., R.H. Verb, T.J. Fischbach, and M.E. Wallace. "A Comparison of Conventional and High Volume-Low Pressure Spray Painting Guns." AIHA Journal. 57:304-310. (1996).
4. Ewert, S.A., S.R. Felstein, and T. Martinez. "Low-Cost Transfer Efficiency Paint Spray Painting Equipment" Metal Finishing. 91(8):59-64. (1993)
5. Lefebvre, A.H. Atomization and Sprays. Hemisphere Publishing Corporation, New York. (1989).
6. Triplett, T. The HVLP Way to Spray. Industrial Paint and Powder. 72(2): 40-41.
7. Kim, K.Y., and Marshall, W.R. "Drop-Size Distributions from Pneumatic Atomizers." AIChE J. 17(3):575-584. (1971).
8. McCabe, W.L, J.C. Smith, and P. Harriot. Unit Operations of Chemical Engineering. McGraw-Hill Book Company. New York. (1985).
9. White, F.M. Fluid Mechanics. McGraw-Hill, Inc. New York. (1994).
10. Schlichting, H. Boundary Layer Theory. McGraw-Hill Book Company. New York. (1979).
11. Baturin, V.V. Fundamentals of Industrial Ventilation. Pergamon Press. New York. (1972).
12. Hinds, W.C. Aerosol Technology: Properties, Behavior, and Measurement of Airborne Particles. John Wiley & Sons. New York. (1992).
13. Carlton, G.N and M.R. Flynn. "A Field Evaluation of an Empirical-Conceptual Model to Predict a Worker's Exposure" Submitted for publication to Appl. Occup. Environ. Hyg.
14. Snowdan-Swan, L. and P. Worner. "Determining Transfer Efficiency and VOC Emissions." Metal Finishing. 91(6):73-78. (1993).
15. Roobol, N.R. Industrial Painting: Principles and Practices. Hitchcock Publishing Co. Carol Stream, IL. p. 259. (1991).
16. Cohen, B.S., and S.V. Hering. Air Sampling Instruments for Evaluation of Atmospheric Contaminants. ACGIH. Cincinnati, Ohio. pp. 283 & 284. (1995).

APPENDIX A: Instrument Calibration, Experimental Results, and Sample Calculations

A.1. Calibration of Alnor Hot Wire Anemometer

A low velocity wind tunnel was constructed in order to calibrate an Alnor hot wire anemometer. The calibration wind tunnel was designed to meet the requirements for testing air flow meters as outlined in the Ventilation Manual (ACGIH, 1995). The components of the calibration wind tunnel included 1) a testing section consisting of a wind tunnel with a cross-sectional area of 2.54 ft^2; 2) a 3.5" diameter orifice meter that served as the air metering device; and 3) an inline damper that served as a means of regulating air flow.

The orifice meter was calibrated using a pitot tube and a manometer. Two pitot traverses perpendicular to one another were made across the diameter of the duct. At each sampling port, six traverse points across the 4" duct were made. Figure A.1 shows the orifice meter calibration, and the equation for the curve is given by the following equation:

$$Q = 275.23\sqrt{h} + 24.82, \qquad r^2 = 0.9993 \tag{A1}$$

where

Q = Air flow across the orifice meter in cfm
h = Pressure drop across the orifice meter in inches of water.

The Alnor hot wire anemometer was calibrated against the orifice meter using this equation. Eight different pressure drops that spanned the working range of the orifice meter manometer were selected. At each pressure setting, the velocity in the calibration wind tunnel was measured with the Alnor anemometer. Figure A.2 shows the calibration curve, with the best fit equation as follows:

$$u' = 1.0848u - 9.5625, \qquad r^2 = 0.999 \tag{A2}$$

where

u = velocity of Alnor anemometer in fpm
u' = "true" velocity in fpm.

A.2. Wind Tunnel Calibration

The wind tunnel was 5-feet-by-5 feet with a resulting cross-sectional area of 25 square feet. The depth of the wind tunnel was 8 feet. The wind tunnel velocity was adjusted by varying the speed of the fan drawing air through the tunnel. Air passing through the pegboard at the rear wall of the tunnel created a measurable static pressure drop relative to atmospheric pressure. This static pressure drop was measured with a pitot tube located in the tunnel exhaust just behind the pegboards and in front of the fan. At eight different static pressures, sixteen measurements of the normal velocity components were taken at a distance of 50 inches from the wind tunnel entrance. Table A.1 summarizes these measurements. The velocity was found to be proportional to the square root of the tunnel static pressure drop as illustrated in Figure A.3, and the following equation is given for the calibration curve:

$$u = 403.75\sqrt{SP_{hood}} - 14.27, \qquad r^2 = 0.9995 \tag{A3}$$

where

u = Velocity in the wind tunnel in fpm
SP_{hood} = Static pressure in the wind tunnel in inches of water.

A.3. Determination of Mass Flowrate of Liquid and Air

The air mass flow rate (m_a) was calibrated with a primary standard spirometer. The air nozzle could be adjusted to change the fan pattern of the liquid spray. Calibration of the air mass was made at three different fan patterns, corresponding to turns on the knob controlling the fan patterns. The calibration curve is seen in Figure A.4 for various knob settings. The following best fit equation corresponds to the fan pattern selected for this experiment (i.e., "2 turns"):

$$Q_{gun} = 1.0076 p_t + 5.1589, \qquad r^2 = 0.986 \tag{A4}$$

where

Q_{gun} = volumetric flowrate of air from the gun in cfm.
p_t = nozzle pressure, based on cap and horn pressure, in psig.

The mass flowrate from the gun was then determined from the product of the volumetric flowrate and the density of air.

The pressure in Equation A4 was based on the pressure from the gun and the nozzle. An air cap tester was used to measured the pressure in both the caps and the horn of the HVLP spray gun. Table A.2 relates the air pressure readings at the pressure gauge to the air pressure measured at the horns and cap.

Liquid was fed to the spray gun from a pressurized tank. The liquid pressure on this tank remained relatively constant at 10 to 11 psig. The liquid mass flowrate (m_l) was determined by comparing the weight of the container before and after spraying.

A.4. Vacuum Pump Oil Viscosity

The liquid viscosity was measured with a Haake falling ball viscometer and constant temperature bath. The results are shown in Figure A.5. The best fit regression equation is as follows:

$$\mu_l = 6.78.95 \; e^{0.00306(T_l)}, \qquad r^2 = 0.9988 \tag{A5}$$

where

μ_l = liquid viscosity in cp
T_l = liquid temperature in °F.

A.5. Experimental Data

The process data for the 63 experimental runs are presented in Table A.3. Measured flowrates and calculated data for the transfer efficiency are given in Table A.4.

A.6. Sample Calculations for Run Number 1

A.6.1 Calculation of m_a/m_l

The measured value of m_a at p_a = 1.5 psig was 131 g/min.

$$m_l = \frac{mass\ \ bucket\ \ (before)\ -\ mass\ \ bucket\ \ (after)}{sampling\ \ time}$$

$$= \frac{(3472.6\ -\ 1948.9)g}{611.78\ \ \text{sec}}\ x\ \left(\frac{60\ \ \text{sec}}{\text{min}}\right)$$

$$= 145.9\ \ g/\text{min}$$

$$\frac{m_a}{m_l} = \frac{131\ \ g/\text{min}}{145.9\ \ g/\text{min}} = 0.9$$

A.6.2 Calculation of Transfer Efficiency

$$TE = \frac{mass\ \ trough\ \ (before)\ -\ mass\ \ trough\ \ (after)}{mass\ \ bucket\ \ (before)\ -\ mass\ \ bucket\ \ (after)}$$

$$= \frac{(1538.7\ -\ 240.0)g}{(3472.6\ -\ 1948.9)g}$$

$$= 0.873$$

A.7. References

American Conference of Governmental Industrial Hygienist. 1995. *Industrial Ventilation: A Manual of Recommended Practices, 22ed.* ACGIH. Cincinnati, Ohio

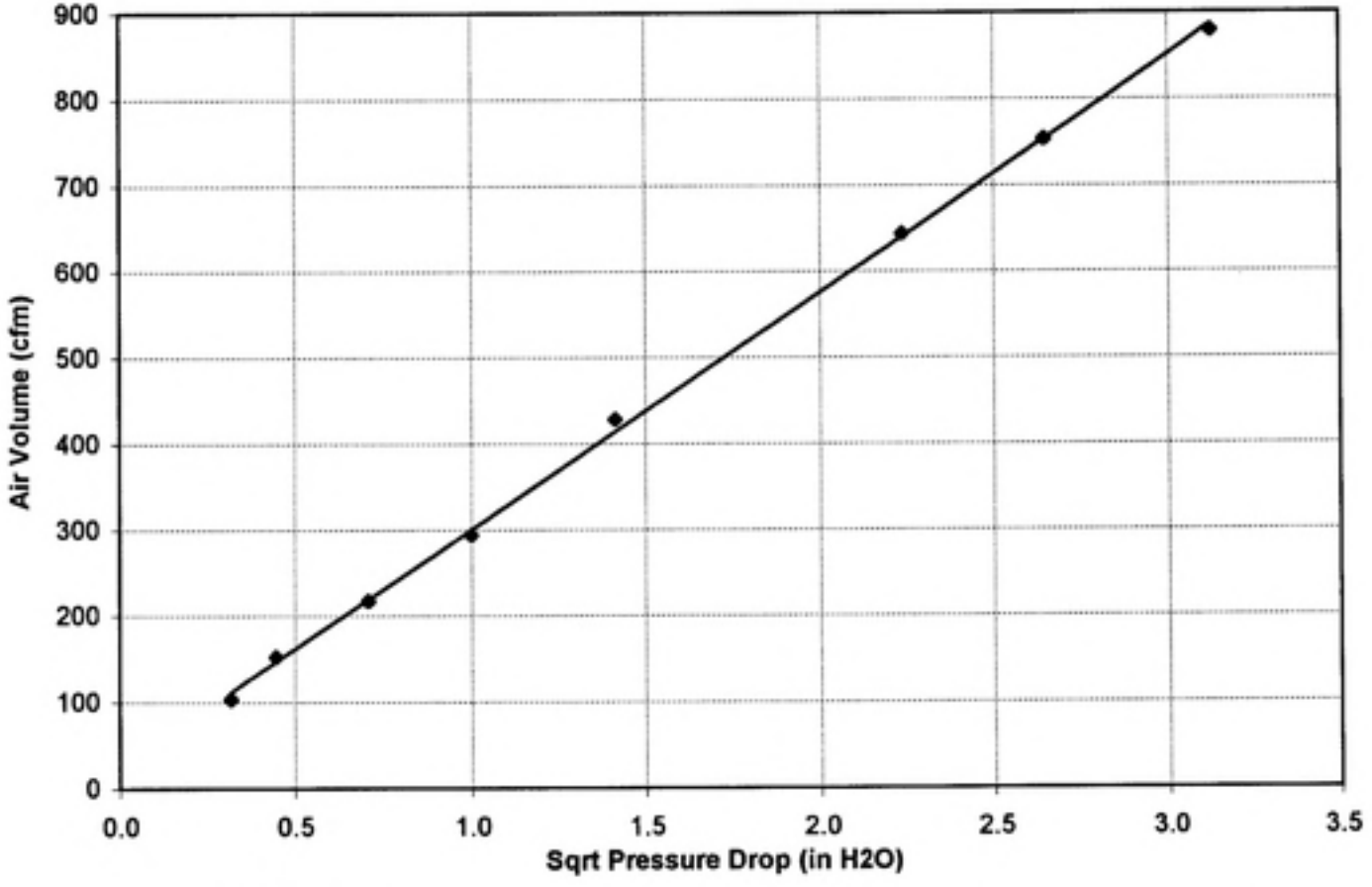

Figure A.1 Air Flow Volume As Function of Square Root of Pressure Drop Across Orifice

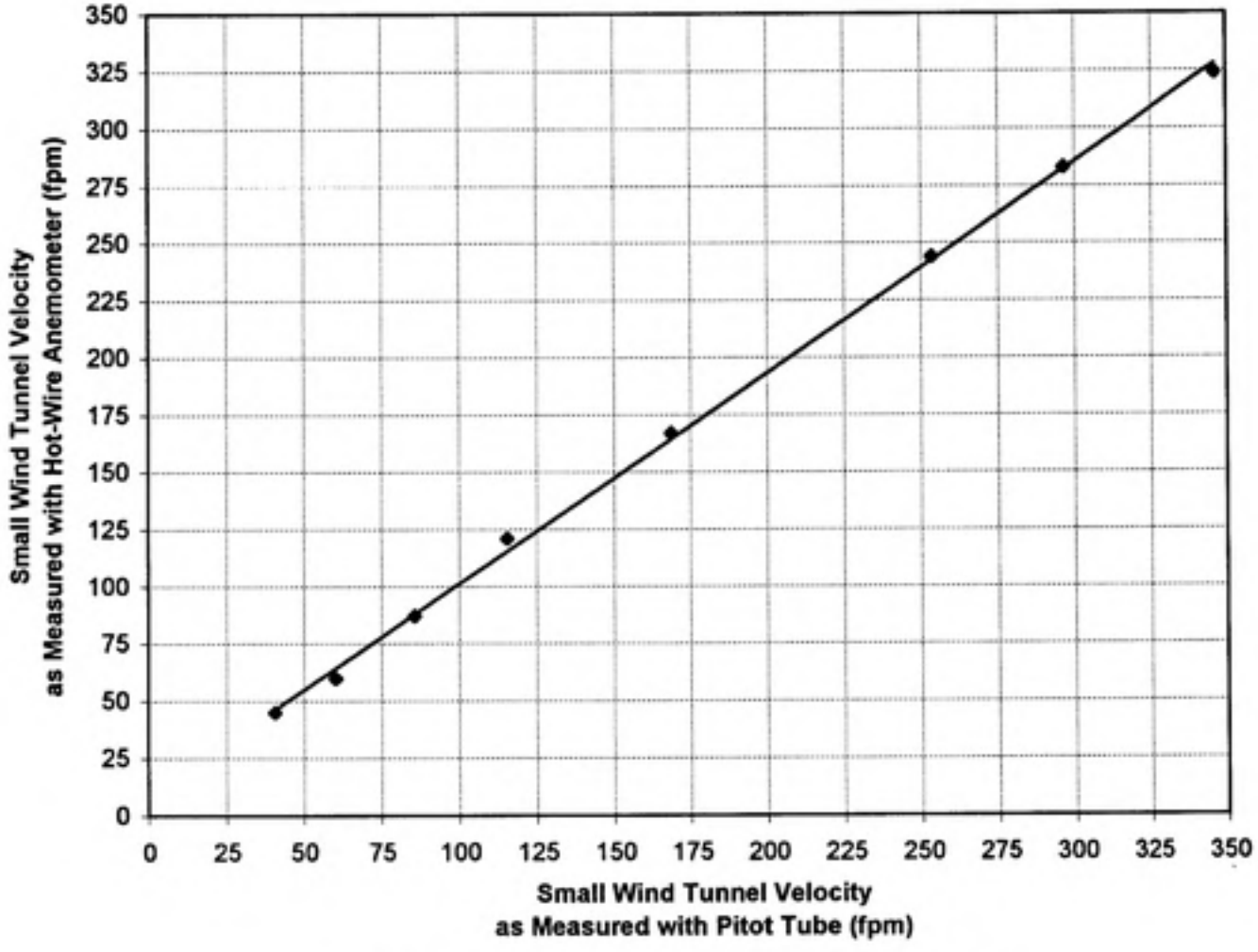

Figure A.2 Calibration of Hot-Wire Anemometer

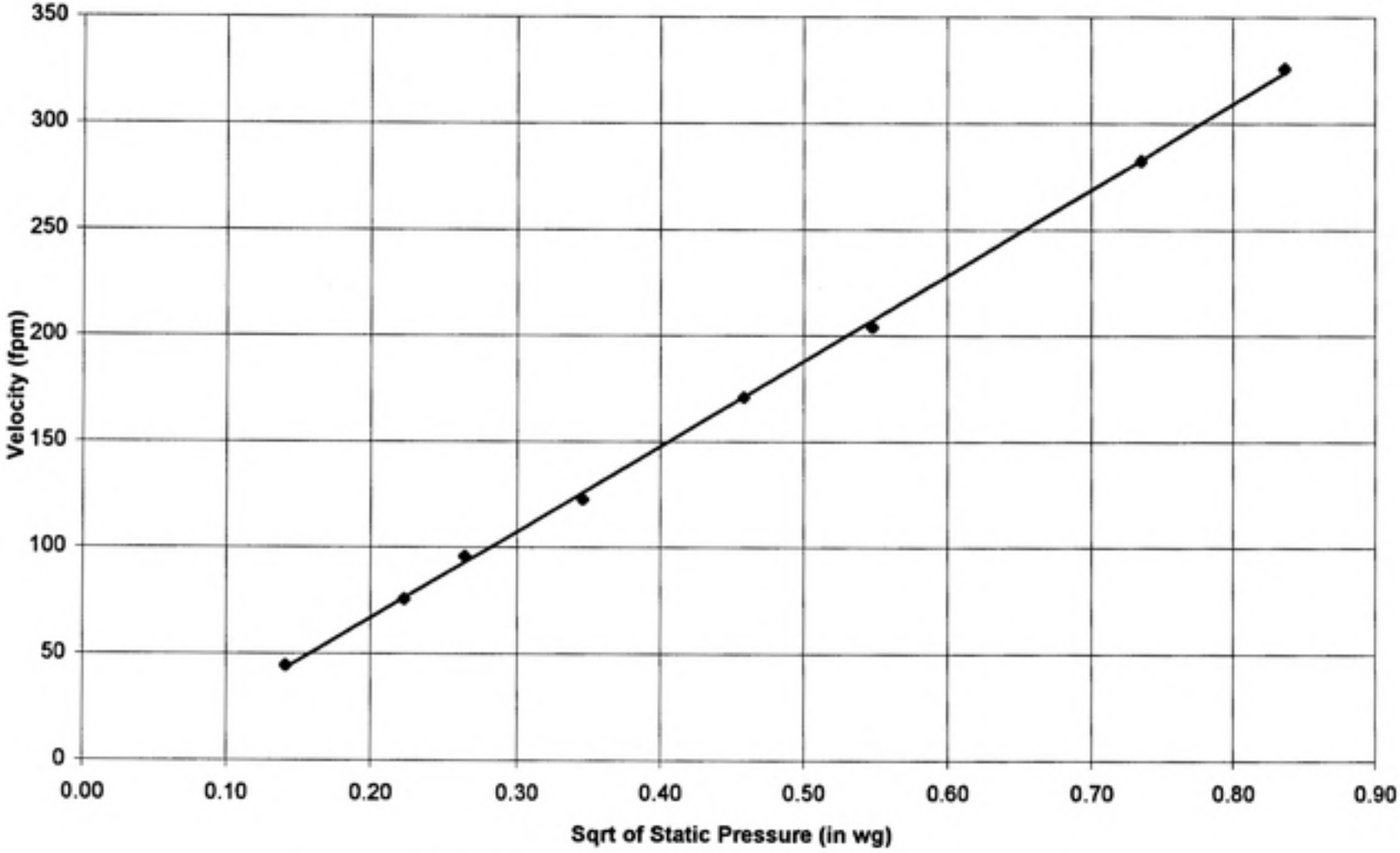

Figure A.3 Calibration of Wind Tunnel Using Hot Wire Anemometer

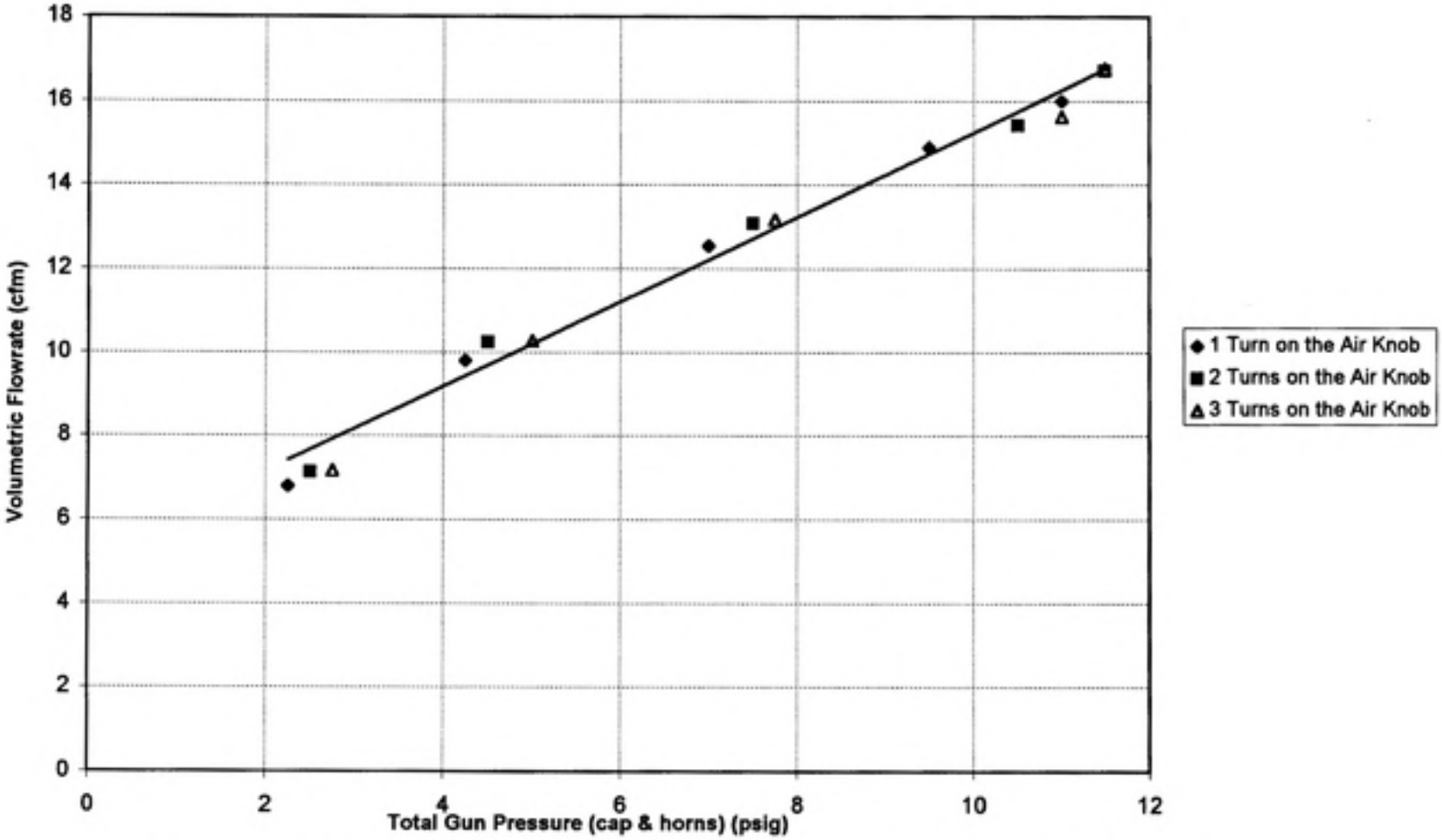

Figure A.4 Air Volumetric Flowrate from the HVLP Gun as a Function of Fan Pattern and Nozzle Pressure

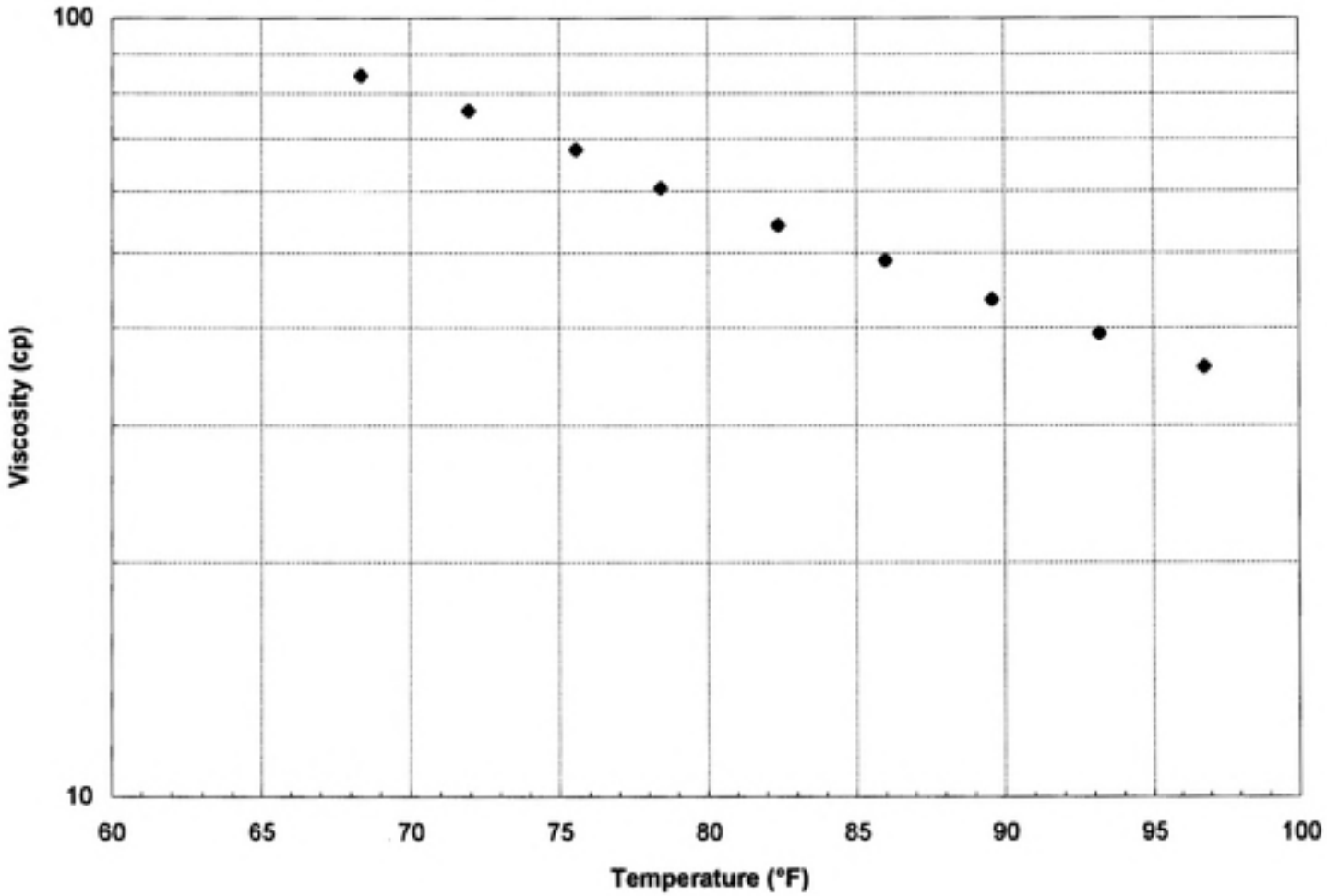

Figure A.5 Viscosity of Vacuum Pump Oil as a Function of Temperature

F

Table A.1 Wind Tunnel Freestream Velocity Profiles (fpm)

Static Pressure of Wind Tunnel (psig) =			0.7
312	313	310	316
311	314	304	321
315	316	302	297
310	306	298	302
Average Velocity (fpm) =		309	

Static Pressure of Wind Tunnel (psig) =			0.54
250	273	279	279
277	277	279	261
274	274	262	260
272	276	260	256
Average Velocity (fpm) =		269	

Static Pressure of Wind Tunnel (psig) =			0.3
182	182	204	204
205	200	203	201
200	203	201	186
198	196	192	197
Average Velocity (fpm) =		197	

Static Pressure of Wind Tunnel (psig) =			0.21
153	165	173	173
169	170	171	166
169	170	167	162
164	166	163	160
Average Velocity (fpm) =		166	

Table A.1 Wind Tunnel Freestream Velocity Profiles (fpm)

Static Pressure of Wind Tunnel (psig) =			0.12
120	122	126	124
124	119	122	111
128	126	120	113
127	124	120	125
Average Velocity (fpm) =		122	

Static Pressure of Wind Tunnel (psig) =			0.07
99	97	95	98
96	95	99	99
96	99	101	88
102	100	95	93
Average Velocity (fpm) =		97	

Static Pressure of Wind Tunnel (psig) =			0.05
77	75	76	84
77	79	80	82
80	78	82	75
80	82	75	75
Average Velocity (fpm) =		79	

Static Pressure of Wind Tunnel (psig) =			0.02
48	43	49	50
54	51	52	54
52	49	51	53
44	48	51	47
Average Velocity (fpm) =		50	

Table A.2 Determination of Air Pressure at the Cap and the Horns

Gauge Pressure (psig)	Number of Turns on Air Knob	Pressure in Cap (psig)	Pressure in Horns (psig)
53	0	10	0
53	1	7	4
53	2	6.5	5
53	3	6.5	5
46	0	8	0
46	1	6	3.5
46	2	6	4.5
46	3	6	5
38	0	6	0
38	1	4.25	2.25
38	2	4.25	3.25
38	3	4.5	3.5
27	0	4	0
27	1	2.75	1.5
27	2	2.5	2.0
27	3	3.0	2.0
16	0	2	0
16	1	1.75	0.75
16	2	1.5	1.0
16	3	1.75	1.0

Table A.3 Process Measurements

Run Number	Static Pressure (in wg)	Freestream Velocity (fpm)	Liquid Temp (F)	Viscosity	Relative Humidity %	Air Temp (F)	Gauge Pressure (psig)	Cap Pressure (psig)	Cap & Horn Pressure (psig)	Orientation	Motion
1	0.16	150.3	81	56.94	62	81	16	1.5	2.5	90°	NO
2	0.12	126.8	81	56.94	62	81	27	2.5	4.5	90°	NO
3	0.08	99.0	81	56.94	62	81	38	4.25	7.5	90°	NO
4	0.048	71.1	81	56.94	62	81	46	6	10.5	90°	NO
5	0.048	71.1	81	56.94	62	81	53	6.5	11.5	90°	NO
6	0.16	150.3	79	60.53	79	76	16	1.5	2.5	180°	NO
7	0.12	126.8	79	60.53	79	76	27	2.5	4.5	180°	NO
8	0.08	99.0	79	60.53	79	76	36	4.25	7.5	180°	NO
9	0.048	71.1	79	60.53	79	76	46	6	10.5	180°	NO
10	0.048	71.1	79	60.53	79	76	53	6.5	11.5	180°	NO
11	0.055	77.8	78	62.41	64	79	53	6.5	11.5	180°	NO
12	0.048	71.1	78	62.41	64	79	46	6	10.5	180°	NO
13	0.08	99.0	78	62.41	64	79	38	4.25	7.5	180°	NO
14	0.12	126.8	78	62.41	64	79	27	2.5	4.5	180°	NO
15	0.16	150.3	78	62.41	64	79	16	1.5	2.5	180°	NO
16	0.16	150.3	78	62.41	64	79	16	1.5	2.5	90°	NO
17	0.12	126.8	78	62.41	64	79	27	2.5	4.5	90°	NO
18	0.08	99.0	78	62.41	64	79	38	4.25	7.5	90°	NO
19	0.048	71.1	78	62.41	64	79	46	6	10.5	90°	NO
20	0.048	71.1	78	62.41	64	79	53	6.5	11.5	90°	NO
21	0.16	150.3	77	64.35	68	77	53	6.5	11.5	90°	NO
22	0.05	73.0	77	64.35	68	77	53	6.5	11.5	90°	NO
23	0.05	73.0	77	64.35	68	77	46	6	10.5	90°	NO
24	0.08	99.0	77	64.35	68	77	38	4.25	7.5	90°	NO
25	0.123	128.7	77	64.35	68	77	27	2.5	4.5	90°	NO
26	0.16	150.3	77	64.35	68	77	16	1.5	2.5	90°	NO
27	0.16	150.3	79	60.53	58	82	16	1.5	2.5	180°	NO
28	0.12	126.8	79	60.53	58	82	27	2.5	4.5	180°	NO
29	0.08	99.0	79	60.53	58	82	38	4.25	7.5	180°	NO
30	0.05	73.0	79	60.53	58	82	46	6	10.5	180°	NO

Table A.3 Process Measurements

Run Number	Static Pressure (in wg)	Freestream Velocity (fpm)	Liquid Temp (F)	Viscosity	Relative Humidity %	Air Temp (F)	Gauge Pressure (psig)	Cap Pressure (psig)	Cap & Horn Pressure (psig)	Orientation	Motion
31	0.05	73.0	79	60.53	58	82	53	6.5	11.5	180°	NO
32	0.16	150.3	80	58.71	58	80	16	1.5	2.5	90°	NO
33	0.12	126.8	80	58.71	58	80	27	2.5	4.5	90°	NO
34	0.12	126.8	80	58.71	58	80	27	2.5	4.5	180°	NO
35	0.08	99.0	80	58.71	58	80	38	4.25	7.5	180°	NO
36	0.08	99.0	80	58.71	58	80	38	4.25	7.5	180°	NO

Table A.3 Process Measurements

Run Number	Static Pressure (in wg)	Freestream Velocity (fpm)	Liquid Temp (F)	Viscosity	Relative Humidity %	Air Temp (F)	Gauge Pressure (psig)	Cap Pressure (psig)	Cap & Horn Pressure (psig)	Orientation	Motion
101	0.16	150.3	75	68.41	47	75	16	1.5	2.5	180°	YES
102	0.12	126.8	75	68.41	47	75	27	2.5	4.5	180°	YES
103	0.08	99.0	75	68.41	47	75	38	4.25	7.5	180°	YES
104	0.05	73.0	75	68.41	47	75	46	6	10.5	180°	YES
105	0.05	73.0	75	68.41	47	75	53	6.5	11.5	180°	YES
106	0.08	99.0	75	68.41	47	75	38	4.25	7.5	90°	YES
107	0.12	126.8	75	68.41	47	75	27	2.5	4.5	90°	YES
108	0.16	150.3	75	68.41	47	75	16	1.5	2.5	90°	YES
109	0.1	113.6	76	66.35	51	76	53	6.5	11.5	90°	YES
110	0.08	99.0	76	66.35	51	76	38	4.25	7.5	90°	YES
111	0.12	126.8	76	66.35	51	76	27	2.5	4.5	90°	YES
112	0.16	150.3	76	66.35	51	76	16	1.5	2.5	90°	YES
113	0.1	113.6	77	64.35	56	77	53	6.5	11.5	180°	YES
114	0.1	113.6	77	64.35	56	77	53	6.5	11.5	180°	YES
115	0.08	99.0	77	64.35	56	77	38	4.25	7.5	180°	YES
116	0.12	126.8	77	64.35	56	77	27	2.5	4.5	180°	YES
117	0.16	150.3	77	64.35	56	77	16	1.5	2.5	180°	YES
118	0.16	150.3	77	64.35	56	77	16	1.5	2.5	180°	YES
119	0.12	126.8	77	64.35	56	77	27	2.5	4.5	180°	YES
120	0.08	99.0	77	64.35	56	77	38	4.25	7.5	180°	YES
121	0.1	113.6	75	68.41	70	75	53	6.5	11.5	180°	YES
122	0.1	113.6	75	68.41	70	75	53	6.5	11.5	180°	YES
123	0.12	126.8	75	68.41	70	75	27	2.5	4.5	180°	YES
124	0.16	150.3	75	68.41	70	75	16	1.5	2.5	90°	YES
125	0.12	126.8	75	68.41	70	75	27	2.5	4.5	90°	YES
126	0.08	99.0	75	68.41	70	75	38	4.25	7.5	90°	YES
127	0.1	113.6	75	68.41	70	75	53	6.5	11.5	90°	YES

Table A.4 Measured Flowrates and Calculated Transfer Efficiencies

Run Number	Run Time (s)	Bucket Weight (g)		Trough Weight (g)		Mass of Liquid Sprayed (g/min)	Mass of Liquid Transferred (g/min)	Mass of Liquid Overspray (m_o) (g/min)	Mass of Air (g/min)**	m_a/m_l	Transfer Efficiency	τ_2 (sec)
		Before	After	Before	After							
1	611.78	3472.6	1984.9	240	1538.7	145.9	127.4	18.5	131	0.9	0.873	5.5E-6
2	610.58	3281.6	1796.4	241.3	1509.4	145.9	124.6	21.3	165	1.1	0.854	3.3E-6
3	302.64	3167.7	2543.8	241.7	741	123.7	99.0	24.7	216	1.8	0.800	1.9E-6
4	303.25	3316.5	2678.9	239.4	733	126.2	97.7	28.5	268	2.1	0.774	1.4E-6
5	304.41	3048.4	2376.8	235.7	750.3	132.4	101.4	30.9	285	2.2	0.766	1.3E-6
6	602.65	3428.5	2203.1	208.5	1277.2	122.0	106.4	15.6	131	1.1	0.872	5.8E-6
7	303.92	3223.9	2596.3	255.5	780.1	123.9	103.6	20.3	165	1.3	0.836	3.5E-6
8	303.12	3139.6	2510.1	235.3	737.9	124.6	99.5	25.1	216	1.7	0.798	2.1E-6
9	303	3411	2760.4	240.6	743.1	128.8	99.5	29.3	268	2.1	0.772	1.5E-6
10	303.89	3251.1	2571.2	251.7	761.8	134.2	100.7	33.5	285	2.1	0.750	1.3E-6
11	305.27	3399.9	2709.5	223	738	135.7	101.2	34.5	285	2.1	0.746	1.4E-6
12	301.4	3211.1	2650.4	236.1	655.3	111.6	83.5	28.2	268	2.4	0.748	1.5E-6
13	303.76	3062.8	2517.3	241.9	668.1	107.7	84.2	23.6	216	2.0	0.781	2.1E-6
14	303.85	3587.6	2976.3	241.6	748	120.7	100.0	20.7	165	1.4	0.828	3.6E-6
15	602.35	3484.3	2312.4	239.9	1260.8	116.7	101.7	15.0	131	1.1	0.871	6.0E-6
16	603.15	3304.6	2108.6	243.8	1289.2	119.0	104.0	15.0	131	1.1	0.874	6.0E-6
17	304.11	3615.7	3052.3	244.2	717.7	111.2	93.4	17.7	165	1.5	0.840	3.6E-6
18	184.03	3525.1	3189.9	244.2	508.2	109.3	86.1	23.2	216	2.0	0.788	2.1E-6
19	183.83	3448	3094.5	249.8	524.4	115.4	89.6	25.8	268	2.3	0.777	1.5E-6
20	183.5	3376.1	3020.9	242.2	502.2	116.1	85.0	31.1	285	2.5	0.732	1.4E-6
21	188.31	3296.6	2934.2	215.3	476.9	115.5	83.4	32.1	285	2.5	0.722	1.4E-6
22	187.5	3174.2	2810.7	236.6	507.9	116.3	86.8	29.5	285	2.5	0.746	1.4E-6
23	188.44	3349.2	3008	244.2	505.4	108.6	83.2	25.5	268	2.5	0.766	1.6E-6
24	182.87	3269	2944.8	244.2	501.7	106.4	84.5	21.9	216	2.0	0.794	2.2E-6
25	303.63	3204.2	2690.6	242	671.9	101.5	85.0	16.5	165	1.6	0.837	3.7E-6
26	603.45	3113.8	2145.3	247.7	1088.3	96.3	83.6	12.7	131	1.4	0.868	6.2E-6
27	602.9	3866.4	2788.5	225.1	1152.7	107.3	92.3	15.0	131	1.2	0.861	5.8E-6

** Mass of air from cap only

Table A.4 Measured Flowrates and Calculated Transfer Efficiencies

Run Number	Run Time (s)	Bucket Weight (g)		Trough Weight (g)		Mass of Liquid Sprayed (g/min)	Mass of Liquid Transferred (g/min)	Mass of Liquid Overspray (m_o) (g/min)	Mass of Air (g/min)**	m_a/m_l	Transfer Efficiency	τ_2 (sec)
		Before	After	Before	After							
28	303.36	3697.6	3136.1	243.3	702.9	111.1	90.9	20.2	165	1.5	0.819	3.5E-6
29	182.34	3595.6	3241.7	242.2	517.5	116.5	90.6	25.9	216	1.9	0.778	2.1E-6
30	189.91	3511	3133.2	243	525.4	119.4	89.2	30.1	268	2.2	0.747	1.5E-6
31	193.04	3414	3009.2	244.5	542.4	125.8	92.6	33.2	285	2.3	0.736	1.3E-6
32	602.94	3698.3	2572.3	207.6	1170.6	112.1	95.8	16.2	131	1.2	0.855	5.7E-6
33	302.27	3497.1	2887.6	242.5	753.1	121.0	101.4	19.6	165	1.4	0.838	3.4E-6
34	182.31	3390.7	2985.9	249.3	589.5	133.2	112.0	21.3	165	1.2	0.840	3.4E-6
35	198.84	3330.2	2903	245.1	585.6	128.9	102.7	26.2	216	1.7	0.797	2.0E-6
36	182.1	3242.3	2823.4	246.1	585.2	138.0	111.7	26.3	216	1.6	0.810	2.0E-6

** Mass of air from cap only

Table A.4 Measured Flowrates and Calculated Transfer Efficiencies

Run Number	Run Time (s)	Bucket Weight (g)		Trough Weight (g)		Mass of Liquid Sprayed (g/min)	Mass of Liquid Transferred (g/min)	Mass of Liquid Overspray (m_o) (g/min)	Mass of Air (g/min)**	m_a/m_l	Transfer Efficiency	τ_2 (sec)
		Before	After	Before	After							
101	603.67	3626	2578	212.9	1097.2	104.2	87.9	16.3	131	1.3	0.844	6.6E-6
102	303	3924	3380.8	213.4	639.1	107.6	84.3	23.3	165	1.5	0.784	4.0E-6
103	182.64	3779.5	3447.7	240.6	485.9	109.0	80.6	28.4	216	2.0	0.739	2.3E-6
104	182.04	3693.4	3375.4	239.9	471.6	104.8	76.4	28.4	268	2.6	0.729	1.6E-6
105	183.81	3617.9	3305.9	227.2	431.9	101.8	66.8	35.0	285	2.8	0.656	1.5E-6
106	182.8	3423.5	3104.8	242.5	470.6	104.6	74.9	29.7	216	2.1	0.716	2.3E-6
107	302.73	3338.5	2819.7	236.8	658.7	102.8	83.6	19.2	165	1.6	0.813	4.0E-6
108	603.08	3240.2	2213.9	237.8	1121.7	102.1	87.9	14.2	131	1.3	0.861	6.6E-6
109	182.11	3528.5	3182.7	235.9	501.2	113.9	87.4	26.5	285	2.5	0.767	1.5E-6
110	222	3442.2	3036.1	241.2	555.8	109.8	85.0	24.7	216	2.0	0.775	2.3E-6
111	304.56	3354.6	2821.6	233.8	666.6	105.0	85.3	19.7	165	1.6	0.812	3.8E-6
112	602.04	3243	2265.8	242.1	1072.9	97.4	82.8	14.6	131	1.3	0.850	6.4E-6
113	181.5	3349.7	2999.6	211.1	451.1	115.7	79.3	36.4	285	2.5	0.686	1.4E-6
114	199.58	3651.8	3255.9	234.1	508.5	119.0	82.5	36.5	285	2.4	0.693	1.4E-6
115	182.3	3520	3160.8	243.9	510.3	118.2	87.7	30.5	216	1.8	0.742	2.2E-6
116	300.3	3433.9	2863.1	236.8	693.3	114.0	91.2	22.8	165	1.4	0.800	3.7E-6
117	604.4	3311.2	2302.9	244.9	1102.7	100.1	85.2	14.9	131	1.3	0.851	6.2E-6
118	618.75	3619.8	2586.1	242.2	1121.5	100.2	85.3	15.0	131	1.3	0.851	6.2E-6
119	303.31	3464.9	2927.1	242.3	666.8	106.4	84.0	22.4	165	1.6	0.789	3.7E-6
120	181.73	3350	3010.4	243.7	496.6	112.1	83.5	28.6	216	1.9	0.745	2.2E-6
121	182.84	3772.9	3432.1	211.1	445.1	111.8	76.8	35.0	285	2.5	0.687	1.5E-6
122	188.63	3639.9	3285.2	237.4	481.8	112.8	77.7	35.1	285	2.5	0.689	1.5E-6
123	304.29	3515.7	3002.7	233.1	635.9	101.2	79.4	21.7	165	1.6	0.785	4.0E-6
124	604.92	3399.3	2426.5	238.7	1069.9	96.5	82.4	14.0	131	1.4	0.854	6.6E-6
125	303.87	3551.4	3045.5	241.5	650.6	99.9	80.8	19.1	165	1.7	0.809	4.0E-6
126	183.85	3458.3	3138.9	237.3	485.3	104.2	80.9	23.3	216	2.1	0.776	2.3E-6
127	184.73	3392.8	3036.5	231.4	484.9	115.7	82.3	33.4	285	2.5	0.711	1.5E-6

** Mass of air from cap only

APPENDIX B: Summary of Statistical Methods

B.1. Determination of Outliers and Normality of Transfer Efficiency

The SAS statistical package was used to test for the presence of outliers in the data set and for the normality of the transfer efficiency. Figure B.1 contains a plot of the transfer efficiency. As seen in the figure, transfer efficiency is normally distributed.

The presence of outliers was determined from a test of the jackknife residual, which is also referred to as a studentized residual without current observation. The jackknife was used because this statistical test detects outliers among the observations (i.e., the transfer efficiencies). Based on 63 observations and two independent variables (discussed below), the critical value for the jackknife is approximately 3.5 (Kleinbaum, et. al., 1988). The highest calculated jackknife was based 2.32, as shown in Figure B.2. Although this value was less than the critical value, the data point was removed from the data set because a measured weight may have been recorded improperly.

B.2. Regression Equation for Transfer Efficiency

An analysis of variance (ANOVA) was used to determine the significance of motion and orientation on transfer efficiency. The ANOVA was also used to determine if the interaction of orientation and motion on transfer efficiency was significant. The results of the ANOVA are presented in Table B.1. As seen in the table, the effect of motion was significant at the 0.05 level ($p=0.0402$), while the effect of orientation was not significant ($p=0.6951$). The interactive effect of motion and orientation was also insignificant at the 0.05 level ($p= 0.6202$). Because motion was shown to be significant, the model of transfer efficiency included the effect of motion.

Dummy variable regression was used to test the significance of the model for transfer efficiency. Table B.2 shows the results of the regression. As seen in the table, the slopes for "Motion" and "No motion" were significantly different at the 0.05 level

(p=0.0039), while the intercepts were not significant (p=0.0859). Tables B.3 and B.4 contain the confidence intervals for the slopes and intercepts categorized by "Motion" and "No motion," respectively.

B.3. Modeled Transfer Efficiency

A regression equation was determined for the measured transfer efficiency as a function of the predicted transfer efficiency. Table B.3 presents the results of the regression equation. Based on the calculated 95% confidence intervals, the slope is statistically different than 1 ($p<0.001$) and the intercept is non-zero (p=0.0003).

B.4. References

Kleinbaum, D.G., L.L. Kupper, and K.E. Muller. 1988. Applied Regression Analysis and Other Multivarialbe Methods. Duxbury Press. Belont, California.

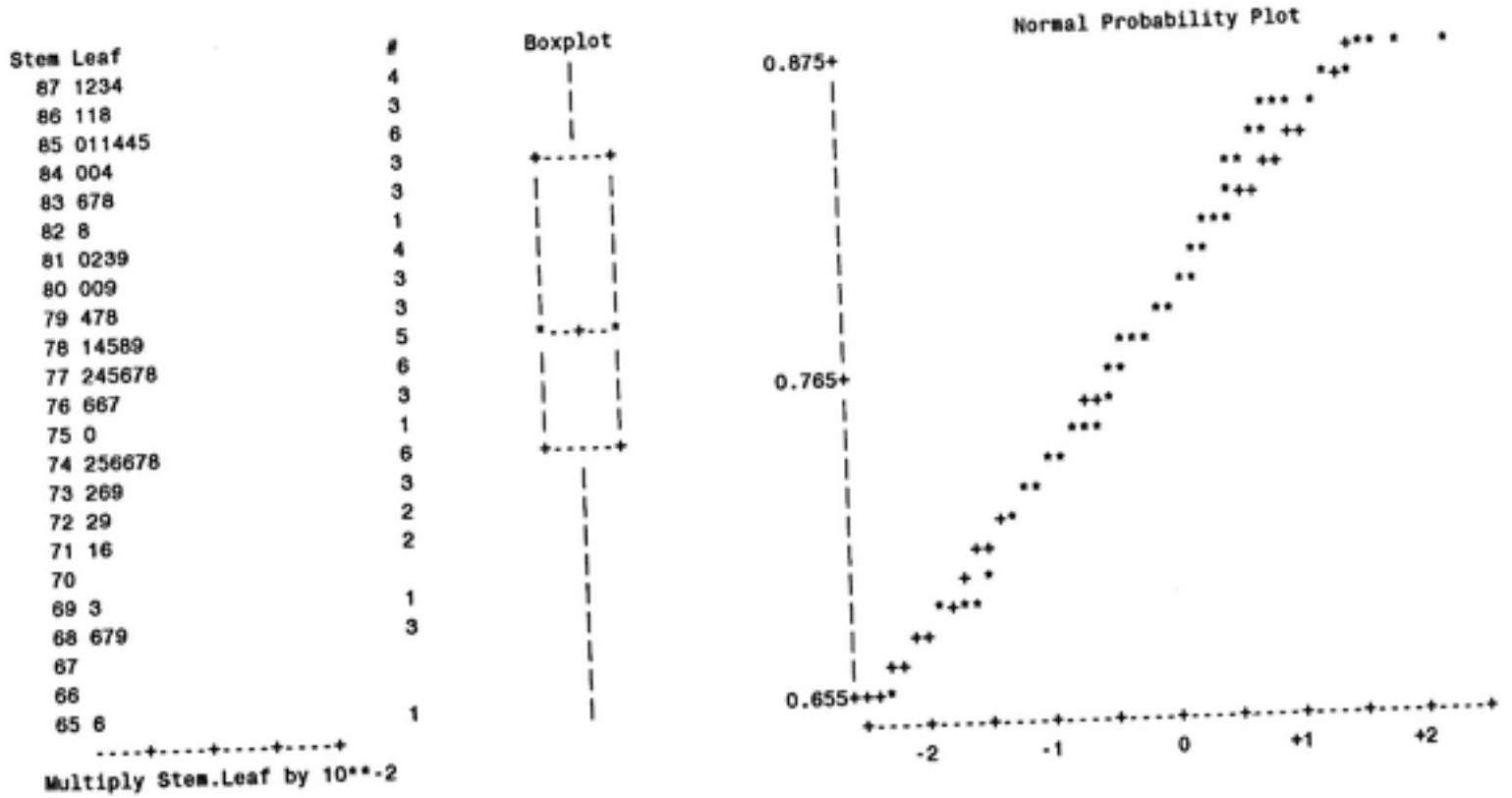

Figure B.1. Normality Plot of Transfer Efficiency

Variable=JKKNIFE Studentized Residual without Current Obs

Moments

N	63	Sum Wgts	63
Mean	0.006465	Sum	0.407282
Std Dev	1.033959	Variance	1.069071
Skewness	0.690646	Kurtosis	0.96227
USS	66.28504	CSS	66.28241
CV	15993.7	Std Mean	0.130267
T:Mean=0	0.049627	Pr>|T|	0.9606
Num ^= 0	63	Num > 0	32
M(Sign)	0.5	Pr>=|M|	1.0000
Sgn Rank	-47	Pr>=|S|	0.7504
W:Normal	0.965252	Pr<W	0.1723

Quantiles(Def=5)

100% Max	3.579912	99%	3.579912
75% Q3	0.695192	95%	1.643758
50% Med	0.01426	90%	1.445598
25% Q1	-0.81976	10%	-1.18989
0% Min	-2.01879	5%	-1.30088
		1%	-2.01879
Range	5.598697		
Q3-Q1	1.514956		
Mode	0.910158		

Extremes

Lowest	Obs	Highest	Obs
-2.01879(	46)	1.563804(	34)
-1.68655(	53)	1.643758(	60)
-1.47259(	38)	1.806877(	31)
-1.30088(	6)	1.877488(	40)
-1.26706(	51)	3.579912(	63)

```
Stem Leaf                #  Boxplot
   3 6                   1     0
   3                           |
   2                           |
   2                           |
   1 56689               5     |
   1 34                  2     |
   0 556677899999        12  +-----+
   0 001222233344        12  *--+--*
  -0 100                 3   |     |
  -0 99988777666666555   17  +-----+
  -1 33221000            8     |
  -1 75                  2     |
  -2 0                   1     |
     ----+----+----+----+
```

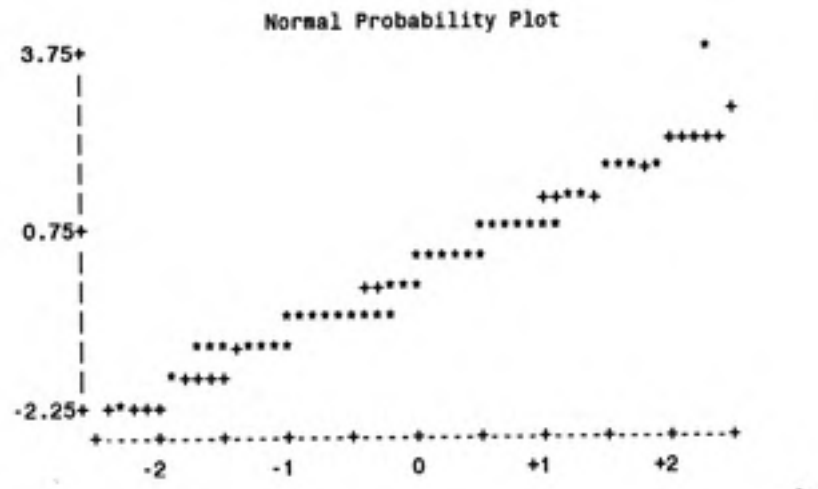

Figure B.2. Summary of Jackknife Residual Diagnostic

Table B.1. Results of ANOVA to Determine the Significance of Motion and Orientation

General Linear Models Procedure

Dependent Variable: TE

Source	DF	Sum of Squares	Mean Square	F Value	Pr > F
Model	3	0.01607324	0.00535775	1.79	0.1592
Error	58	0.17365123	0.00299399		
Corrected Total	61	0.18972447			

R-Square	C.V.	Root MSE	TE Mean
0.084719	6.931764	0.05471733	0.78937097

Source	DF	Type I SS	Mean Square	F Value	Pr > F
MOTION	1	0.01504895	0.01504895	5.03	0.0288
ORIENT	1	0.00028127	0.00028127	0.09	0.7603
MOTION*ORIENT	1	0.00074302	0.00074302	0.25	0.6202

Source	DF	Type III SS	Mean Square	F Value	Pr > F
MOTION	1	0.01319096	0.01319096	4.41	0.0402
ORIENT	1	0.00046468	0.00046468	0.16	0.6951
MOTION*ORIENT	1	0.00074302	0.00074302	0.25	0.6202

Table B.2. Dummy Variable Regression for Transfer Efficiency Model

General Linear Models Procedure

Dependent Variable: TE

Source	DF	Sum of Squares	Mean Square	F Value	Pr > F
Model	3	0.17164233	0.05721411	183.52	0.0001
Error	58	0.01808214	0.00031176		
Corrected Total	61	0.18972447			

R-Square	C.V.	Root MSE	TE Mean
0.904693	2.236813	0.01765676	0.78937097

Source	DF	Type I SS	Mean Square	F Value	Pr > F
MAML	1	0.16244634	0.16244634	521.06	0.0001
MOTION	1	0.00638105	0.00638105	20.47	0.0001
MAML*MOTION	1	0.00281494	0.00281494	9.03	0.0039

Source	DF	Type III SS	Mean Square	F Value	Pr > F
MAML	1	0.15633258	0.15633258	501.45	0.0001
MOTION	1	0.00095167	0.00095167	3.05	0.0859
MAML*MOTION	1	0.00281494	0.00281494	9.03	0.0039

Parameter		Estimate	T for H0: Parameter=0	Pr > |T|	Std Error of Estimate
INTERCEPT		0.9955423795 B	71.20	0.0001	0.01398275
MAML		-.1201049767 B	-16.57	0.0001	0.00724747
MOTION	N	-.0312082785 B	-1.75	0.0859	0.01786233
	Y	0.0000000000 B	.	.	.
MAML*MOTION	N	0.0284195021 B	3.00	0.0039	0.00945785
	Y	0.0000000000 B	.	.	.

Table B.3 Calculation fo Confidence Intervals for Transfer Efficiency as a Function of Mass Ratio and No Motion

Regression Statistics	
Multiple R	0.958
R Square	0.917
Adjusted R Square	0.914
Standard Error	0.014
Observations	36

ANOVA

	df	*SS*	*MS*	*F*	*Significance F*
Regression	1	0.071139368	0.071139	374.7066	6.19331E-20
Residual	34	0.006455019	0.00019		
Total	35	0.077594387			

	Coefficients	*Standard Error*	*t Stat*	*P-value*	*Lower 95%*	*Upper 95%*
Intercept	0.966	0.008726385	110.6538	4.5E-45	0.948	0.983
Slope of Regression Line	-0.093	0.004792854	-19.3573	6.19E-20	-0.103	-0.083

Table B.4 Calculation fo Confidence Intervals for Transfer Efficiency as a Function of Mass Ratio and Motion

Regression Statistics	
Multiple R	0.949
R Square	0.901
Adjusted R Square	0.897
Standard Error	0.020
Observations	26

ANOVA

	df	*SS*	*MS*	*F*	*Significance F*
Regression	1	0.087557858	0.087558	217.974	1.53279E-13
Residual	24	0.009640546	0.000402		
Total	25	0.097198404			

	Coefficients	*Standard Error*	*t Stat*	*P-value*	*Lower 95%*	*Upper 95%*
Intercept	0.998	0.015890632	62.82397	3.84E-28	0.966	1.031
Slope of Regression Line	-0.122	0.008261439	-14.7639	1.53E-13	-0.139	-0.105

Table B.5 Regression Statistics for Measured Transfer Efficiency as a Function of Predicted Transfer Efficiency: No Motion

Regression Statistics	
Multiple R	0.976
R Square	0.952
Adjusted R Square	0.950
Standard Error	0.010
Observations	36

ANOVA

	df	*SS*	*MS*	*F*	*Significance F*
Regression	1	0.073861353	0.073861	672.7198	5.50864E-24
Residual	34	0.003733034	0.00011		
Total	35	0.077594387			

	Coefficients	*Standard Error*	*t Stat*	*P-value*	*Lower 95%*	*Upper 95%*
Intercept	0.108	0.026827993	4.036259	0.000292	0.054	0.163
Slope of Regression Line	0.852	0.032841634	25.93684	5.51E-24	0.785	0.919

APPENDIX C. Calculation of Transfer Efficiency from the Inertial Impaction Model

This appendix presents sample calculations for the inertial impaction model. Sample calculations were based on experimental run number 1. Table C.1 presents the measured experimental parameters, intermediate calculations, and the resulting estimations for transfer efficiencies for the impaction model.

C.1. Calculation of Areas for HVLP Spray Gun

$$A_{cap} = \pi \left[\left(\frac{0.193\ in}{2} \times \frac{ft}{12\ in} \right)^2 - \left(\frac{0.098\ in}{2} \times \frac{ft}{12\ in} \right)^2 + 2\left(\frac{0.038\ in}{2} \times \frac{ft}{12\ in} \right)^2 \right]$$

$$= 1.67x10^{-4}\ ft^2$$

$$A_{horns} = 2\pi \left[\left(\frac{0.12\ in}{2} \times \frac{ft}{12\ in} \right)^2 + \left(\frac{0.056\ in}{2} \times \frac{ft}{12\ in} \right)^2 \right]$$

$$= 1.91x10^{-4}\ ft^2$$

$$A_{liq} = \pi \left(\frac{0.098\ in}{2} \times \frac{ft}{12\ in} \right)^2$$

$$= 5.24x10^{-5}\ ft^2$$

C.2 Determining Mass Flowrate of Air from Cap and Horns

The mass flowrate of air from the cap and the horns was estimated as the product of air velocity as given in Equation 2, air density, and area of air discharge. Table C.2 contains the comparison between measured air mass flowrates and those calculated from the velocity. The cap pressure for run number 1 was 1.5 psi.

$$u_{cap} = \left[\frac{2\ \gamma\ g_c\ p_o}{(\gamma - 1)\rho_o} \left[1 - \left(\frac{p}{p_o} \right)^{(1-1/\gamma)} \right] \right]^{0.5}$$

$$= \left[\frac{2 \times 1.4 \times (32.174\, ft \cdot lb_m / lb_f \cdot s^2)(14.696 + 1.5)psi}{(1.4 - 1) \times (0.08 lb_m / ft^3)} \times \left(\frac{12^2 in^2}{ft^2} \right) \times \right]^{0.5}$$
$$\left[1 - \left(\frac{1.5 psi}{(14.696 + 6.5) psi} \right)^{(1-1/1.4)} \right]$$

$$= 423\ \ ft/s$$

$$m_a = A_{cap}\ \ \rho_{air}\ \ u_{cap}$$
$$= (1.67 x 10^{-4}\ \ ft^2)(0.075 lb/ft^3)(423\ \ ft/s)\left(60 s/\text{min}\right)$$
$$= 0.32\ \ lb/\text{min}$$

C.3. Calculation of Mass Median Diameter of Particle Size Distribution

C.3.1 Estimation of relative velocity

The total pressure of the air gun was calculated as 1.5 psig at the cap plus 1 psig at the horns. The mass of liquid spray was calculated as 145.9 g/min in Appendix A.

$$Q_{cap} = (1.0076\ \ p_t\ + \ 5.1589) \times 0.5$$
$$Q_{cap} = (1.0076\ \ [(1.5+1)\ \ psig]\ + \ 5.1589) \times 0.5$$
$$= 3.85\ \ cfm$$

$$U_{air} = \frac{Q_{cap}}{A_{cap}} = \frac{3.85\ \ cfm}{1.67x10^{-4}\ ft^2} \times \left(\frac{\min}{60s}\right)$$

$$= 384.2\ \ ft/s$$

$$U_{liq} = \frac{m_{liq}}{\rho_{liq}\ \ A_{liq}} = \frac{145.9\ \ gpm \times \left(\frac{lb_m}{454g}\right)}{(53.6\ \ lb_m/ft^3)\ \ (5.24x10^{-5}\ ft^2)} \times \left(\frac{\min}{60\sec}\right)$$

$$= 1.9\ \ ft/s$$

$$U_{rel} = U_{air} - U_{liq}$$

$$= (384.2\ \ ft/s) - (1.9\ \ ft/s)$$

$$= 382.2\ \ ft/s$$

C.3.2. Calculation of surface tension of liquid

Surface tension of the vacuum pump oil was not available from the manufacturer. Instead, the surface tension was calculated from a formula given in *Perry's Chemical Engineers' Handbook* (1984). This formula estimates surface tension from parachor values, which are based on the chemical structure of a given compound and are calculated by summing values assigned to the functional groups in the compound. The vacuum pump oil is a paraffin wax composed of methyl groups $(-CH_2-)_n$, where n ranges from 20 to 40. An n of 30 was used to estimate the surface tension. The structural contribution for the $(-CH_2-)$ was 40.3 and 55.5 for $(-CH_3)$. Additionally, in the surface tension equation, the density of the compound in its gas phase was ignored.

$$\sigma^{\frac{1}{4}} = \left[Parachor\ \ value\right] \times \left[(\rho_{liq} - \rho_{gas})mol/cm^3\right]$$

$$\sigma = \left[\left[28*40.3 + 2*55.5\right] \times \left[\frac{0.86\ \ g/cm^3}{422\ \ g/mol}\right]\right]^4$$

$$= 40.7\ \ dynes/cm$$

C.3.3 Calculation of MMD

The mass median diameter for run number 1 was calculated from Equation 1. Input for the equation were based on measured values and calculated values previously noted.

$$MMD = 249\left[\frac{\sigma^{0.41}\ \mu_l^{0.32}}{\left(v_{rel}^2\ \rho_a\right)^{0.57} A^{0.36} \rho_l^{0.16}}\right] + 1260\left(\frac{\mu_l^2}{\rho_l\ \sigma}\right)^{0.17} \frac{1}{v_{rel}^{0.54}} \left(\frac{m_a}{m_l}\right)^m$$

$$= 249\left[\frac{(40.7\ \ dynes/cm)^{0.41}(56.9\ \ cp)^{0.32}}{\left((382.2\ \ ft/s)^2(0.075\ \ lb/ft^3)\right)^{0.57}(1.67x10^{-4}\ \ ft^2)^{0.36}(53.7\ \ lb/ft^3)^{0.16}}\right] +$$

$$1260\left(\frac{56.9\ \ cp^2}{(53.7\ \ lb/ft^3)(40.7\ \ dynes/cm)}\right)^{0.17} \frac{1}{(382.2\ \ ft/s)_l^{0.54}} \left(\frac{131g/\min}{145.9g/\min}\right)^{-1}$$

$$= 102.5\ \ \mu m$$

C.4. Calculation of Velocity at Hypothetical Nozzle

C.4.1 Calculation of distance to hypothetical jet

The distance from the hypothetical jet to the workpiece (Y) was calculated from basic trigonometry, given the spray pattern of particles on the workpiece and the spray angle from the hypothetical jet. The fan pattern from the HVLP was a 2:1 ellipse, approximately 9 inches in length.

$$A_{ellipse} = \pi(a)(b) = \pi\left(\frac{9\ in}{2}\right)\left(\frac{4.5\ in}{2}\right) = 31.8\ in^2$$

$$r_{eq} = \left(\frac{A_{ellipse}}{\pi}\right)^{0.5} = \left(\frac{31.8\ in^2}{\pi}\right)^{0.5} = 3.2\ in$$

$$Y = \left(\frac{r_{eq}}{\tan\theta}\right) = \left(\frac{3.2\ in}{\tan\left(\frac{29°}{2}\right)}\right) = \left(\frac{3.2\ in}{0.26}\right) = 12.3\ in$$

C.4.2 Calculation of distance from hypothetical jet and calculation of hypothetical nozzle diameter

The distance from the hypothetical jet to the hypothetical nozzle depended on the diameter of the hypothetical nozzle. As a constraint, the diameter and the distance from the nozzle to the workpiece were set equal, and the lengths were determined from iterative calculations.

$$X = \frac{radius\ of\ nozzle}{\tan\left(\frac{\theta}{2}\right)}$$

$$= \frac{D_{nozzle}/2\ in}{\tan\left(\frac{29°}{2}\right)}$$

$$D_{nozzle} = (Y - X) = (12.3\ in - X)$$

Solving iteratively

$D_{nozzle} = 4.2\ in$ *and* $X = 8.1\ in$

C.4.3 Calculation of velocity at hypothetical jet

The momentum from the hypothetical jet was assumed to equal the momentum from the HVLP spray gun. The total mass of air from the spray gun was used, and the velocity was based on the total discharge area (cap and horns). The total pressure was 2.5 psig for run number 1.

$$\begin{aligned} Q_{gun} &= \left(1.0076 p_t + 5.1589\right) \\ &= \left(1.0076 \left(2.5 psig\right) + 5.1589\right) \\ &= 7.68 \ cfm \end{aligned}$$

$$\begin{aligned} m_a &= Q_{gun} \ \rho_a \\ &= (7.68 \ cfm) \times (0.075 \ lb_m / ft^3) \times \left(\frac{454g}{lb_m}\right) \times \left(\frac{kg}{1000g}\right) \times \left(\frac{\min}{60s}\right) \\ &= 4.36x10^{-3} \ kg / s \end{aligned}$$

$$\begin{aligned} U_{gun} &= \frac{Q_{gun}}{A_{(cap + horn)}} \\ &= \frac{7.83 \ cfm}{\left(1.67x10^{-4} + 1.91x10^{-4}\right) ft^2} \times \left(\frac{m}{3.2808 ft}\right) \times \left(\frac{\min}{60s}\right) \\ &= 109.0 \ m / s \end{aligned}$$

The velocity of the hypothetical impactor was determined from the volumetric flowrate of the jet calculated from Equation 3 and the diameter of the hypothetical nozzle.

$$Q_{jet} = 0.404 \; x \; \sqrt{K} = 0.404 \; x \; \sqrt{\frac{m_{gun} \; U_{gun}}{\rho_a}}$$

$$= 0.404 \left[(8.1 \; in) \times \left(\frac{2.54 \; cm}{in} \right) \times \left(\frac{m}{100 \; cm} \right) \right] \sqrt{\frac{(4.36x10^{-3} \; kg/s)(109.0 \; m/s)}{1.2 \; kg/m^3}}$$

$$= 0.052 \; m^3/s$$

$$U_{nozzle} = \frac{Q_{nozzle}}{A_{nozzle}} = \frac{Q_{nozzle}}{\pi \; (D_{nozzle}/2)^2}$$

$$= \frac{0.052 \; m^3/s}{\pi \left(\frac{4.2 \; in}{2} \right)^2} \times \left(\frac{12^2 \; in^2}{ft^2} \right) \times \left(\frac{(3.2808)^2 \; ft^2}{m^2} \right)$$

$$= 5.87 \; m/s$$

C.5. Calculation of Cut Size Diameter for Hypothetical Nozzle

The cut size for the hypothetical impactor was calculated using Equation 4.

$$d_{50} = \left[\frac{9 \; \mu_a \; D_{nozzle} \; (STK_{50})}{\rho_p \; U_{nozzle} \; C_c} \right]^{0.5}$$

$$= \left[\frac{9 \; (1.81x10^{-5} cp) \; (0.1065)m \; (0.24)}{(861 \; kg/m^3) \; (5.87 \; m/s) \; 1} \right]^{0.5}$$

$$= 2.886x10^{-5} m = 2.886x10^{-5} \times \left(\frac{1{,}000{,}000 \; \mu m}{m} \right)$$

$$= 28.86 \; \mu m$$

C.6. Calculation of Transfer Efficiency

The overspray was calculated from Equation 5.

$$x^* = \left(\frac{d_{50}}{MMD}\right)$$

$$= \left(\frac{28.86 \ \mu m}{102.5 \ \mu m}\right)$$

$$= 0.28$$

$$\Phi_v = \frac{1.15}{1 + 6.67 \exp\left(-2.18 \ x^*\right)} - 0.15$$

$$= \frac{1.15}{1 + 6.67 \exp\left(-2.18 \times 0.28\right)} - 0.15$$

$$= 0.10$$

$$TE_{pred} = 1 - \Phi_v = 1 - 0.1$$

$$= 0.90$$

C.7. References

Perry, R.H., D.W. Green., and J.O. Maloney. 1984. *Perry's Chemical Engineers' Handbook: Sixth Edition*. McGraw-Hill Book Company. New York.

Table C.1 Calculated Results for Inertial Impaction Model

	Process Measurements									
Run Number	Orientation	Motion	T_{lab}		T_{oil}	P_{HVLP} *Cap*	P_{HVLP} *Cap + Horn*	$U_{wind\ tunnel}$	$m_{vp\ oil}$	Measured Transfer Efficiency
			(°F)	(°K)	(°F)	(psig)	(psig)	(fpm)	(g/min)	
1	90°	NO	81.0	300.4	81.0	1.5	2.5	150.3	145.91	0.87
2	90°	NO	81.0	300.4	81.0	2.5	4.5	126.8	145.95	0.85
3	90°	NO	81.0	300.4	81.0	4.5	7.5	99.0	123.69	0.80
4	90°	NO	81.0	300.4	81.0	6	10.5	71.1	126.15	0.77
5	90°	NO	81.0	300.4	81.0	6.5	11.5	71.1	132.37	0.77
6	180°	NO	76.0	297.6	79.0	1.5	2.5	150.3	122.00	0.87
7	180°	NO	76.0	297.6	79.0	2.5	4.5	126.8	123.90	0.84
8	180°	NO	76.0	297.6	79.0	4.5	7.5	99.0	124.60	0.80
9	180°	NO	76.0	297.6	79.0	6	10.5	71.1	128.83	0.77
10	180°	NO	76.0	297.6	79.0	6.5	11.5	71.1	134.24	0.75
11	180°	NO	79.0	299.3	78.0	6.5	11.5	77.8	135.70	0.75
12	180°	NO	79.0	299.3	78.0	6	10.5	71.1	111.62	0.75
13	180°	NO	79.0	299.3	78.0	4.5	7.5	99.0	107.75	0.78
14	180°	NO	79.0	299.3	78.0	2.5	4.5	126.8	120.71	0.83
15	180°	NO	79.0	299.3	78.0	1.5	2.5	150.3	116.73	0.87
16	90°	NO	79.0	299.3	78.0	1.5	2.5	150.3	118.98	0.87
17	90°	NO	79.0	299.3	78.0	2.5	4.5	126.8	111.16	0.84
18	90°	NO	79.0	299.3	78.0	4.5	7.5	99.0	109.29	0.79
19	90°	NO	79.0	299.3	78.0	6	10.5	71.1	115.38	0.78
20	90°	NO	79.0	299.3	78.0	6.5	11.5	71.1	116.14	0.73
21	90°	NO	77.0	298.2	77.0	6.5	11.5	150.3	115.47	0.72
22	90°	NO	77.0	298.2	77.0	6.5	11.5	73.0	116.32	0.75
23	90°	NO	77.0	298.2	77.0	6	10.5	73.0	108.64	0.77
24	90°	NO	77.0	298.2	77.0	4.5	7.5	99.0	106.37	0.79
25	90°	NO	77.0	298.2	77.0	2.5	4.5	128.7	101.49	0.84
26	90°	NO	77.0	298.2	77.0	1.5	2.5	150.3	96.30	0.87
27	180°	NO	82.0	301.0	79.0	1.5	2.5	150.3	107.27	0.86
28	180°	NO	82.0	301.0	79.0	2.5	4.5	126.8	111.06	0.82
29	180°	NO	82.0	301.0	79.0	4.5	7.5	99.0	116.45	0.78

Table C.1 Calculated Results for Inertial Impaction Model

Run Number	*Process Measurements*									
	Orientation	Motion	T_{lab}		T_{oil}	P_{HVLP} *Cap*	P_{HVLP} *Cap + Horn*	$U_{wind\ tunnel}$	$m_{vp\ oil}$	Measured Transfer Efficiency
			(°F)	(°K)	(°F)	(psig)	(psig)	(fpm)	(g/min)	
30	180°	NO	82.0	301.0	79.0	6	10.5	73.0	119.36	0.75
31	180°	NO	82.0	301.0	79.0	6.5	11.5	73.0	125.82	0.74
32	90°	NO	80.0	299.9	80.0	1.5	2.5	150.3	112.05	0.86
33	90°	NO	80.0	299.9	80.0	2.5	4.5	126.8	120.98	0.84
34	180°	NO	80.0	299.9	80.0	2.5	4.5	126.8	133.22	0.84
35	180°	NO	80.0	299.9	80.0	4.5	7.5	99.0	128.91	0.80
36	180°	NO	80.0	299.9	80.0	4.5	7.5	99.0	138.02	0.81

Table C.1 Calculated Results for Inertial Impaction Model

Run Number	*Spray Characteristics*								
	$A_{air\ (CAP)}$		$A_{air\ (HORN)}$		A_{liquid}		α_{spray}	$X_{gun\text{-}plate}$	
	(in^2)	(m^2)	(in^2)	(m^2)	(in^2)	(m^2)	(degrees)	(in)	(m)
1	2.4E-2	1.5E-5	2.8E-2	1.8E-5	7.5E-3	4.9E-6	42	8	0.2032
2	2.4E-2	1.5E-5	2.8E-2	1.8E-5	7.5E-3	4.9E-6	42	8	0.2032
3	2.4E-2	1.5E-5	2.8E-2	1.8E-5	7.5E-3	4.9E-6	42	8	0.2032
4	2.4E-2	1.5E-5	2.8E-2	1.8E-5	7.5E-3	4.9E-6	42	8	0.2032
5	2.4E-2	1.5E-5	2.8E-2	1.8E-5	7.5E-3	4.9E-6	42	8	0.2032
6	2.4E-2	1.5E-5	2.8E-2	1.8E-5	7.5E-3	4.9E-6	42	8	0.2032
7	2.4E-2	1.5E-5	2.8E-2	1.8E-5	7.5E-3	4.9E-6	42	8	0.2032
8	2.4E-2	1.5E-5	2.8E-2	1.8E-5	7.5E-3	4.9E-6	42	8	0.2032
9	2.4E-2	1.5E-5	2.8E-2	1.8E-5	7.5E-3	4.9E-6	42	8	0.2032
10	2.4E-2	1.5E-5	2.8E-2	1.8E-5	7.5E-3	4.9E-6	42	8	0.2032
11	2.4E-2	1.5E-5	2.8E-2	1.8E-5	7.5E-3	4.9E-6	42	8	0.2032
12	2.4E-2	1.5E-5	2.8E-2	1.8E-5	7.5E-3	4.9E-6	42	8	0.2032
13	2.4E-2	1.5E-5	2.8E-2	1.8E-5	7.5E-3	4.9E-6	42	8	0.2032
14	2.4E-2	1.5E-5	2.8E-2	1.8E-5	7.5E-3	4.9E-6	42	8	0.2032
15	2.4E-2	1.5E-5	2.8E-2	1.8E-5	7.5E-3	4.9E-6	42	8	0.2032
16	2.4E-2	1.5E-5	2.8E-2	1.8E-5	7.5E-3	4.9E-6	42	8	0.2032
17	2.4E-2	1.5E-5	2.8E-2	1.8E-5	7.5E-3	4.9E-6	42	8	0.2032
18	2.4E-2	1.5E-5	2.8E-2	1.8E-5	7.5E-3	4.9E-6	42	8	0.2032
19	2.4E-2	1.5E-5	2.8E-2	1.8E-5	7.5E-3	4.9E-6	42	8	0.2032
20	2.4E-2	1.5E-5	2.8E-2	1.8E-5	7.5E-3	4.9E-6	42	8	0.2032
21	2.4E-2	1.5E-5	2.8E-2	1.8E-5	7.5E-3	4.9E-6	42	8	0.2032
22	2.4E-2	1.5E-5	2.8E-2	1.8E-5	7.5E-3	4.9E-6	42	8	0.2032
23	2.4E-2	1.5E-5	2.8E-2	1.8E-5	7.5E-3	4.9E-6	42	8	0.2032
24	2.4E-2	1.5E-5	2.8E-2	1.8E-5	7.5E-3	4.9E-6	42	8	0.2032
25	2.4E-2	1.5E-5	2.8E-2	1.8E-5	7.5E-3	4.9E-6	42	8	0.2032
26	2.4E-2	1.5E-5	2.8E-2	1.8E-5	7.5E-3	4.9E-6	42	8	0.2032
27	2.4E-2	1.5E-5	2.8E-2	1.8E-5	7.5E-3	4.9E-6	42	8	0.2032
28	2.4E-2	1.5E-5	2.8E-2	1.8E-5	7.5E-3	4.9E-6	42	8	0.2032
29	2.4E-2	1.5E-5	2.8E-2	1.8E-5	7.5E-3	4.9E-6	42	8	0.2032

Table C.1 Calculated Results for Inertial Impaction Model

Run Number	*Spray Characteristics*								
	$A_{air\ (CAP)}$		$A_{air\ (HORN)}$		A_{liquid}		α_{spray}	$X_{gun\text{-}plate}$	
	(in^2)	(m^2)	(in^2)	(m^2)	(in^2)	(m^2)	(degrees)	(in)	(m)
30	2.4E-2	1.5E-5	2.8E-2	1.8E-5	7.5E-3	4.9E-6	42	8	0.2032
31	2.4E-2	1.5E-5	2.8E-2	1.8E-5	7.5E-3	4.9E-6	42	8	0.2032
32	2.4E-2	1.5E-5	2.8E-2	1.8E-5	7.5E-3	4.9E-6	42	8	0.2032
33	2.4E-2	1.5E-5	2.8E-2	1.8E-5	7.5E-3	4.9E-6	42	8	0.2032
34	2.4E-2	1.5E-5	2.8E-2	1.8E-5	7.5E-3	4.9E-6	42	8	0.2032
35	2.4E-2	1.5E-5	2.8E-2	1.8E-5	7.5E-3	4.9E-6	42	8	0.2032
36	2.4E-2	1.5E-5	2.8E-2	1.8E-5	7.5E-3	4.9E-6	42	8	0.2032

Table C.1 Calculated Results for Inertial Impaction Model

	Properties of Air						
Run Number	MW_{air}	γ_{air}	$\Lambda_{any\ ideal\ gas}$	R_{air}	ρ_{air} @ HVLP	ρ_{air} @ HVLP	μ_{air} @ 1 atm
	(kg / kg mole)	C_p/C_v	(kg m^2 / kg mole s^2 °K)	(m^2 / s^2 °K)	(kg/m^3)	(lb/ft^3)	(kg/ms)
1	28.97	1.4	8314	286.99	1.20	7.5E-2	1.8E-5
2	28.97	1.4	8314	286.99	1.20	7.5E-2	1.8E-5
3	28.97	1.4	8314	286.99	1.20	7.5E-2	1.8E-5
4	28.97	1.4	8314	286.99	1.20	7.5E-2	1.8E-5
5	28.97	1.4	8314	286.99	1.20	7.5E-2	1.8E-5
6	28.97	1.4	8314	286.99	1.20	7.5E-2	1.8E-5
7	28.97	1.4	8314	286.99	1.20	7.5E-2	1.8E-5
8	28.97	1.4	8314	286.99	1.20	7.5E-2	1.8E-5
9	28.97	1.4	8314	286.99	1.20	7.5E-2	1.8E-5
10	28.97	1.4	8314	286.99	1.20	7.5E-2	1.8E-5
11	28.97	1.4	8314	286.99	1.20	7.5E-2	1.8E-5
12	28.97	1.4	8314	286.99	1.20	7.5E-2	1.8E-5
13	28.97	1.4	8314	286.99	1.20	7.5E-2	1.8E-5
14	28.97	1.4	8314	286.99	1.20	7.5E-2	1.8E-5
15	28.97	1.4	8314	286.99	1.20	7.5E-2	1.8E-5
16	28.97	1.4	8314	286.99	1.20	7.5E-2	1.8E-5
17	28.97	1.4	8314	286.99	1.20	7.5E-2	1.8E-5
18	28.97	1.4	8314	286.99	1.20	7.5E-2	1.8E-5
19	28.97	1.4	8314	286.99	1.20	7.5E-2	1.8E-5
20	28.97	1.4	8314	286.99	1.20	7.5E-2	1.8E-5
21	28.97	1.4	8314	286.99	1.20	7.5E-2	1.8E-5
22	28.97	1.4	8314	286.99	1.20	7.5E-2	1.8E-5
23	28.97	1.4	8314	286.99	1.20	7.5E-2	1.8E-5
24	28.97	1.4	8314	286.99	1.20	7.5E-2	1.8E-5
25	28.97	1.4	8314	286.99	1.20	7.5E-2	1.8E-5
26	28.97	1.4	8314	286.99	1.20	7.5E-2	1.8E-5
27	28.97	1.4	8314	286.99	1.20	7.5E-2	1.8E-5
28	28.97	1.4	8314	286.99	1.20	7.5E-2	1.8E-5
29	28.97	1.4	8314	286.99	1.20	7.5E-2	1.8E-5

Table C.1 Calculated Results for Inertial Impaction Model

	Properties of Air						
Run Number	MW_{air}	γ_{air}	$\Lambda_{any\ ideal\ gas}$	R_{air}	$\rho_{air\ @\ HVLP}$	$\rho_{air\ @\ HVLP}$	$\mu_{air\ @\ 1\ atm}$
	(kg / kg mole)	C_p/C_v	(kg m^2 / kg mole s^2 °K)	(m^2 / s^2 °K)	(kg/m^3)	(lb/ft^3)	(kg/ms)
30	28.97	1.4	8314	286.99	1.20	7.5E-2	1.8E-5
31	28.97	1.4	8314	286.99	1.20	7.5E-2	1.8E-5
32	28.97	1.4	8314	286.99	1.20	7.5E-2	1.8E-5
33	28.97	1.4	8314	286.99	1.20	7.5E-2	1.8E-5
34	28.97	1.4	8314	286.99	1.20	7.5E-2	1.8E-5
35	28.97	1.4	8314	286.99	1.20	7.5E-2	1.8E-5
36	28.97	1.4	8314	286.99	1.20	7.5E-2	1.8E-5

Table C.1 Calculated Results for Inertial Impaction Model

Run Number	*Properties of Oil*				*Calculation of m_a/m_l*				
	$\rho_{vp\ oil}$	$\rho_{vp\ oil}$ @	$\mu_{vp\ oil}$ @ Tknown	$\sigma_{vp\ oil}$	m_{air} *(Based on Cap Pressure Only)*			$m_{vp\ oil}$	$m_{air}/m_{vp\ oil}$
	(kg/m^3)	(lb/ft^3)	(cp)	(dynes/cm)	(lb/min)	(g/min)	(kg/s)	(kg/s)	(computed)
1	861	53.7	56.9	40.7	0.288	130.72	2.2E-3	2.4E-3	0.9
2	861	53.7	56.9	40.7	0.364	165.03	2.8E-3	2.4E-3	1.1
3	861	53.7	56.9	40.7	0.477	216.49	3.6E-3	2.1E-3	1.8
4	861	53.7	56.9	40.7	0.591	267.95	4.5E-3	2.1E-3	2.1
5	861	53.7	56.9	40.7	0.629	285.11	4.8E-3	2.2E-3	2.2
6	861	53.7	60.5	40.7	0.288	130.72	2.2E-3	2.0E-3	1.1
7	861	53.7	60.5	40.7	0.364	165.03	2.8E-3	2.1E-3	1.3
8	861	53.7	60.5	40.7	0.477	216.49	3.6E-3	2.1E-3	1.7
9	861	53.7	60.5	40.7	0.591	267.95	4.5E-3	2.1E-3	2.1
10	861	53.7	60.5	40.7	0.629	285.11	4.8E-3	2.2E-3	2.1
11	861	53.7	62.4	40.7	0.629	285.11	4.8E-3	2.3E-3	2.1
12	861	53.7	62.4	40.7	0.591	267.95	4.5E-3	1.9E-3	2.4
13	861	53.7	62.4	40.7	0.477	216.49	3.6E-3	1.8E-3	2.0
14	861	53.7	62.4	40.7	0.364	165.03	2.8E-3	2.0E-3	1.4
15	861	53.7	62.4	40.7	0.288	130.72	2.2E-3	1.9E-3	1.1
16	861	53.7	62.4	40.7	0.288	130.72	2.2E-3	2.0E-3	1.1
17	861	53.7	62.4	40.7	0.364	165.03	2.8E-3	1.9E-3	1.5
18	861	53.7	62.4	40.7	0.477	216.49	3.6E-3	1.8E-3	2.0
19	861	53.7	62.4	40.7	0.591	267.95	4.5E-3	1.9E-3	2.3
20	861	53.7	62.4	40.7	0.629	285.11	4.8E-3	1.9E-3	2.5
21	861	53.7	64.4	40.7	0.629	285.11	4.8E-3	1.9E-3	2.5
22	861	53.7	64.4	40.7	0.629	285.11	4.8E-3	1.9E-3	2.5
23	861	53.7	64.4	40.7	0.591	267.95	4.5E-3	1.8E-3	2.5
24	861	53.7	64.4	40.7	0.477	216.49	3.6E-3	1.8E-3	2.0
25	861	53.7	64.4	40.7	0.364	165.03	2.8E-3	1.7E-3	1.6
26	861	53.7	64.4	40.7	0.288	130.72	2.2E-3	1.6E-3	1.4
27	861	53.7	60.5	40.7	0.288	130.72	2.2E-3	1.8E-3	1.2
28	861	53.7	60.5	40.7	0.364	165.03	2.8E-3	1.9E-3	1.5
29	861	53.7	60.5	40.7	0.477	216.49	3.6E-3	1.9E-3	1.9

Table C.1 Calculated Results for Inertial Impaction Model

	Properties of Oil				*Calculation of m_a/m_l*				
Run Number	$\rho_{vp\ oil}$	$\rho_{vp\ oil}$ @	$\mu_{vp\ oil}$ @ T=known	$\sigma_{vp\ oil}$	m_{air} *(Based on Cap Pressure Only)*			$m_{vp\ oil}$	$m_{air}/m_{vp\ oil}$
	(kg/m^3)	(lb/ft^3)	(cp)	(dynes/cm)	(lb/min)	(g/min)	(kg/s)	(kg/s)	(computed)
30	861	53.7	60.5	40.7	0.591	267.95	4.5E-3	2.0E-3	2.2
31	861	53.7	60.5	40.7	0.629	285.11	4.8E-3	2.1E-3	2.3
32	861	53.7	58.7	40.7	0.288	130.72	2.2E-3	1.9E-3	1.2
33	861	53.7	58.7	40.7	0.364	165.03	2.8E-3	2.0E-3	1.4
34	861	53.7	58.7	40.7	0.364	165.03	2.8E-3	2.2E-3	1.2
35	861	53.7	58.7	40.7	0.477	216.49	3.6E-3	2.1E-3	1.7
36	861	53.7	58.7	40.7	0.477	216.49	3.6E-3	2.3E-3	1.6

Table C.1 Calculated Results for Inertial Impaction Model

Run Number	*Calculation of Relative Velocity of Air to Liquid*				
	V_{air} *(Based on Cap Pressure Only)*		$V_{vp\ oil}$	$V_{relative}$	$V_{relative}$
	(ft/min)	(m/s)	(m/s)	(m/s)	(ft/s)
1	23,052	117.11	0.58	116.53	382
2	29,103	147.84	0.58	147.26	483
3	38,179	193.95	0.49	193.46	635
4	47,254	240.06	0.50	239.55	786
5	50,280	255.42	0.53	254.90	836
6	23,052	117.11	0.49	116.62	383
7	29,103	147.84	0.49	147.35	483
8	38,179	193.95	0.50	193.45	635
9	47,254	240.06	0.51	239.54	786
10	50,280	255.42	0.53	254.89	836
11	50,280	255.42	0.54	254.88	836
12	47,254	240.06	0.44	239.61	786
13	38,179	193.95	0.43	193.52	635
14	29,103	147.84	0.48	147.36	483
15	23,052	117.11	0.46	116.64	383
16	23,052	117.11	0.47	116.63	383
17	29,103	147.84	0.44	147.40	484
18	38,179	193.95	0.43	193.52	635
19	47,254	240.06	0.46	239.60	786
20	50,280	255.42	0.46	254.96	836
21	50,280	255.42	0.46	254.96	836
22	50,280	255.42	0.46	254.96	836
23	47,254	240.06	0.43	239.62	786
24	38,179	193.95	0.42	193.53	635
25	29,103	147.84	0.40	147.44	484
26	23,052	117.11	0.38	116.72	383
27	23,052	117.11	0.43	116.68	383
28	29,103	147.84	0.44	147.40	484
29	38,179	193.95	0.46	193.49	635

Table C.1 Calculated Results for Inertial Impaction Model

Run Number	*Calculation of Relative Velocity of Air to Liquid*				
	V_{air} *(Based on Cap Pressure Only)*		$V_{vp\ oil}$	$V_{relative}$	$V_{relative}$
	(ft/min)	(m/s)	(m/s)	(m/s)	(ft/s)
30	47,254	240.06	0.47	239.58	786
31	50,280	255.42	0.50	254.92	836
32	23,052	117.11	0.45	116.66	383
33	29,103	147.84	0.48	147.36	483
34	29,103	147.84	0.53	147.31	483
35	38,179	193.95	0.51	193.44	635
36	38,179	193.95	0.55	193.40	635

Table C.1 Calculated Results for Inertial Impaction Model

	Iterative Calculation for Area of Equivalent Nozzle							
Run Number	$X_{jet\ pole\text{-}plate}$	$X_{nozzle\text{-}plate}$	$X_{jet\ pole\text{-}nozzle}$	$X_{jet\ pole\text{-}nozzle}$	α_{jet}		D_{nozzle}	A_{nozzle}
	(in)	(in)	(in)	(m)	(degrees)	(radians)	(m)	(m^2)
1	12.3	4.19	8.11	0.206	29	0.506	0.1065	8.9E-3
2	12.3	4.19	8.11	0.206	29	0.506	0.1065	8.9E-3
3	12.3	4.19	8.11	0.206	29	0.506	0.1065	8.9E-3
4	12.3	4.19	8.11	0.206	29	0.506	0.1065	8.9E-3
5	12.3	4.19	8.11	0.206	29	0.506	0.1065	8.9E-3
6	12.3	4.19	8.11	0.206	29	0.506	0.1065	8.9E-3
7	12.3	4.19	8.11	0.206	29	0.506	0.1065	8.9E-3
8	12.3	4.19	8.11	0.206	29	0.506	0.1065	8.9E-3
9	12.3	4.19	8.11	0.206	29	0.506	0.1065	8.9E-3
10	12.3	4.19	8.11	0.206	29	0.506	0.1065	8.9E-3
11	12.3	4.19	8.11	0.206	29	0.506	0.1065	8.9E-3
12	12.3	4.19	8.11	0.206	29	0.506	0.1065	8.9E-3
13	12.3	4.19	8.11	0.206	29	0.506	0.1065	8.9E-3
14	12.3	4.19	8.11	0.206	29	0.506	0.1065	8.9E-3
15	12.3	4.19	8.11	0.206	29	0.506	0.1065	8.9E-3
16	12.3	4.19	8.11	0.206	29	0.506	0.1065	8.9E-3
17	12.3	4.19	8.11	0.206	29	0.506	0.1065	8.9E-3
18	12.3	4.19	8.11	0.206	29	0.506	0.1065	8.9E-3
19	12.3	4.19	8.11	0.206	29	0.506	0.1065	8.9E-3
20	12.3	4.19	8.11	0.206	29	0.506	0.1065	8.9E-3
21	12.3	4.19	8.11	0.206	29	0.506	0.1065	8.9E-3
22	12.3	4.19	8.11	0.206	29	0.506	0.1065	8.9E-3
23	12.3	4.19	8.11	0.206	29	0.506	0.1065	8.9E-3
24	12.3	4.19	8.11	0.206	29	0.506	0.1065	8.9E-3
25	12.3	4.19	8.11	0.206	29	0.506	0.1065	8.9E-3
26	12.3	4.19	8.11	0.206	29	0.506	0.1065	8.9E-3
27	12.3	4.19	8.11	0.206	29	0.506	0.1065	8.9E-3
28	12.3	4.19	8.11	0.206	29	0.506	0.1065	8.9E-3
29	12.3	4.19	8.11	0.206	29	0.506	0.1065	8.9E-3

Table C.1 Calculated Results for Inertial Impaction Model

	Iterative Calculation for Area of Equivalent Nozzle							
Run Number	$X_{jet\ pole\text{-}plate}$	$X_{nozzle\text{-}plate}$	$X_{jet\ pole\text{-}nozzle}$	$X_{jet\ pole\text{-}nozzle}$	α_{jet}		D_{nozzle}	A_{nozzle}
	(in)	(in)	(in)	(m)	(degrees)	(radians)	(m)	(m^2)
30	12.3	4.19	8.11	0.206	29	0.506	0.1065	8.9E-3
31	12.3	4.19	8.11	0.206	29	0.506	0.1065	8.9E-3
32	12.3	4.19	8.11	0.206	29	0.506	0.1065	8.9E-3
33	12.3	4.19	8.11	0.206	29	0.506	0.1065	8.9E-3
34	12.3	4.19	8.11	0.206	29	0.506	0.1065	8.9E-3
35	12.3	4.19	8.11	0.206	29	0.506	0.1065	8.9E-3
36	12.3	4.19	8.11	0.206	29	0.506	0.1065	8.9E-3

Table C.1 Calculated Results for Inertial Impaction Model

	Calculation of Velocity from Equivalent Nozzle						*Calculation of Stokes Cut Diameter*					
Run Number	m_{air} *(Based on Cap & Horn)*	U_{air} *(Based on Cap & Horn)*	J_{jet}	K_{jet}	Q_{nozzle}	v_{nozzle}	$\rho_{air\ @\ nozzle}$	Re_{nozzle}	$x_{nozzle-plate}/D_{nozzle}$	C_c	Stk_{50}	d_{50}
	(kg/s)	m/s	(kg m / s^2)	(m^4/s^2)	(m^3/s)	(m/s)	(kg/m^3)					(µm)
1	4.4E-3	109.0	0.475	0.396	5.2E-2	5.87	1.2	4.1E+4	1	1	0.24	28.86
2	5.5E-3	137.6	0.757	0.631	6.6E-2	7.42	1.2	5.2E+4	1	1	0.24	25.68
3	7.2E-3	180.5	1.303	1.086	8.7E-2	9.73	1.2	6.8E+4	1	1	0.24	22.42
4	8.9E-3	223.4	1.996	1.663	1.1E-1	12.04	1.2	8.4E+4	1	1	0.24	20.16
5	9.5E-3	237.8	2.259	1.883	1.1E-1	12.81	1.2	8.9E+4	1	1	0.24	19.54
6	4.4E-3	109.0	0.475	0.396	5.2E-2	5.87	1.2	4.1E+4	1	1	0.24	28.77
7	5.5E-3	137.6	0.757	0.631	6.6E-2	7.42	1.2	5.2E+4	1	1	0.24	25.60
8	7.2E-3	180.5	1.303	1.086	8.7E-2	9.73	1.2	6.8E+4	1	1	0.24	22.35
9	8.9E-3	223.4	1.996	1.663	1.1E-1	12.04	1.2	8.5E+4	1	1	0.24	20.09
10	9.5E-3	237.8	2.259	1.883	1.1E-1	12.81	1.2	9.0E+4	1	1	0.24	19.48
11	9.5E-3	237.8	2.259	1.883	1.1E-1	12.81	1.2	9.0E+4	1	1	0.24	19.52
12	8.9E-3	223.4	1.996	1.663	1.1E-1	12.04	1.2	8.4E+4	1	1	0.24	20.13
13	7.2E-3	180.5	1.303	1.086	8.7E-2	9.73	1.2	6.8E+4	1	1	0.24	22.40
14	5.5E-3	137.6	0.757	0.631	6.6E-2	7.42	1.2	5.2E+4	1	1	0.24	25.65
15	4.4E-3	109.0	0.475	0.396	5.2E-2	5.87	1.2	4.1E+4	1	1	0.24	28.82
16	4.4E-3	109.0	0.475	0.396	5.2E-2	5.87	1.2	4.1E+4	1	1	0.24	28.82
17	5.5E-3	137.6	0.757	0.631	6.6E-2	7.42	1.2	5.2E+4	1	1	0.24	25.65
18	7.2E-3	180.5	1.303	1.086	8.7E-2	9.73	1.2	6.8E+4	1	1	0.24	22.40
19	8.9E-3	223.4	1.996	1.663	1.1E-1	12.04	1.2	8.4E+4	1	1	0.24	20.13
20	9.5E-3	237.8	2.259	1.883	1.1E-1	12.81	1.2	9.0E+4	1	1	0.24	19.52
21	9.5E-3	237.8	2.259	1.883	1.1E-1	12.81	1.2	9.0E+4	1	1	0.24	19.49
22	9.5E-3	237.8	2.259	1.883	1.1E-1	12.81	1.2	9.0E+4	1	1	0.24	19.49
23	8.9E-3	223.4	1.996	1.663	1.1E-1	12.04	1.2	8.4E+4	1	1	0.24	20.10
24	7.2E-3	180.5	1.303	1.086	8.7E-2	9.73	1.2	6.8E+4	1	1	0.24	22.37
25	5.5E-3	137.6	0.757	0.631	6.6E-2	7.42	1.2	5.2E+4	1	1	0.24	25.62
26	4.4E-3	109.0	0.475	0.396	5.2E-2	5.87	1.2	4.1E+4	1	1	0.24	28.78
27	4.4E-3	109.0	0.475	0.396	5.2E-2	5.87	1.2	4.1E+4	1	1	0.24	28.88
28	5.5E-3	137.6	0.757	0.631	6.6E-2	7.42	1.2	5.2E+4	1	1	0.24	25.70
29	7.2E-3	180.5	1.303	1.086	8.7E-2	9.73	1.2	6.8E+4	1	1	0.24	22.44

Table C.1 Calculated Results for Inertial Impaction Model

Run Number	*Calculation of Velocity from Equivalent Nozzle*						*Calculation of Stokes Cut Diameter*					
	m_{air} *(Based on Cap & Horn)*	U_{air} *(Based on Cap & Horn)*	J_{jet}	K_{jet}	Q_{nozzle}	v_{nozzle}	$\rho_{air\ @\ nozzle}$	Re_{nozzle}	$x_{nozzle\text{-}plate}/D_{nozzle}$	C_c	Stk_{50}	d_{50}
	(kg/s)	m/s	(kg m / s^2)	(m^4/s^2)	(m^3/s)	(m/s)	(kg/m^3)					(μm)
30	8.9E-3	223.4	1.996	1.663	1.1E-1	12.04	1.2	8.4E+4	1	1	0.24	20.17
31	9.5E-3	237.8	2.259	1.883	1.1E-1	12.81	1.2	8.9E+4	1	1	0.24	19.55
32	4.4E-3	109.0	0.475	0.396	5.2E-2	5.87	1.2	4.1E+4	1	1	0.24	28.84
33	5.5E-3	137.6	0.757	0.631	6.6E-2	7.42	1.2	5.2E+4	1	1	0.24	25.67
34	5.5E-3	137.6	0.757	0.631	6.6E-2	7.42	1.2	5.2E+4	1	1	0.24	25.67
35	7.2E-3	180.5	1.303	1.086	8.7E-2	9.73	1.2	6.8E+4	1	1	0.24	22.41
36	7.2E-3	180.5	1.303	1.086	8.7E-2	9.73	1.2	6.8E+4	1	1	0.24	22.41

Table C.1 Calculated Results for Inertial Impaction Model

	Calculation of K&M mmd		*Calculation of Theoretical TE*		
Run Number	K&M Exponent for M_a/M_t	mmd	$X^* d_{50}$/mmd	Φ_v	$1-\Phi_v$
		(μm)		oversprayed	transferred
1	-1	102.50	0.28	0.10	0.90
2	-1	74.38	0.35	0.13	0.87
3	-1	47.09	0.48	0.19	0.81
4	-1	35.74	0.56	0.24	0.76
5	-1	33.68	0.58	0.25	0.75
6	-1	94.40	0.30	0.11	0.89
7	-1	69.36	0.37	0.14	0.86
8	-1	48.23	0.46	0.19	0.81
9	-1	36.85	0.55	0.23	0.77
10	-1	34.61	0.56	0.24	0.76
11	-1	35.15	0.56	0.23	0.77
12	-1	34.77	0.58	0.25	0.75
13	-1	45.39	0.49	0.20	0.80
14	-1	69.10	0.37	0.14	0.86
15	-1	93.09	0.31	0.11	0.89
16	-1	94.05	0.31	0.11	0.89
17	-1	66.23	0.39	0.15	0.85
18	-1	45.70	0.49	0.20	0.80
19	-1	35.31	0.57	0.24	0.76
20	-1	32.62	0.60	0.26	0.74
21	-1	32.86	0.59	0.26	0.74
22	-1	32.97	0.59	0.26	0.74
23	-1	34.70	0.58	0.25	0.75
24	-1	45.58	0.49	0.20	0.80
25	-1	63.97	0.40	0.15	0.85
26	-1	85.14	0.34	0.12	0.88
27	-1	88.11	0.33	0.12	0.88
28	-1	65.54	0.39	0.15	0.85
29	-1	46.64	0.48	0.19	0.81

Table C.1 Calculated Results for Inertial Impaction Model

	Calculation of K&M mmd		*Calculation of Theoretical TE*		
Run Number	K&M Exponent for M_a/M_t	mmd	$X^* d_{50}$/mmd	Φ_v	$1-\Phi_v$
		(μm)		overspayed	transferred
30	-1	35.51	0.57	0.24	0.76
31	-1	33.53	0.58	0.25	0.75
32	-1	89.25	0.32	0.12	0.88
33	-1	67.80	0.38	0.14	0.86
34	-1	71.41	0.36	0.13	0.87
35	-1	48.58	0.46	0.18	0.82
36	-1	50.35	0.45	0.18	0.82

Table C.2 Calculated Mass Air Flowrates from the Cap and Horns

Measured Pressure (psig)		Calculated Density in the Reservoir (ρ_o) (lb/ft^3)		Calculated Velocity (ft/s)		Calculated Mass Flowrate (lb/min)			Calculated Fraction of Mass		Measured Flowrate: Cap and Horns		Percent Difference
Cap	Horn	Cap	Horns	Cap	Horns	Cap	Horns	Cap & Horns	Cap	Horns	cfm	lb/min	
1.50	1.00	0.080	0.079	423.05	347.39	0.32	0.30	0.62	0.51	0.49	7.7	0.58	7%
2.50	2.00	0.084	0.082	540.18	485.79	0.40	0.42	0.82	0.49	0.51	9.7	0.73	13%
4.50	3.25	0.091	0.086	710.00	611.05	0.53	0.53	1.06	0.50	0.50	13.0	0.97	9%
6.00	4.50	0.096	0.091	808.19	710.00	0.61	0.61	1.22	0.50	0.50	15.7	1.18	3%
6.50	5.00	0.097	0.092	837.34	744.77	0.63	0.64	1.27	0.49	0.51	16.7	1.26	1%